Kufner, S.-K., Schurr, B., Ratschbacher, L., Murodkulov, S., Abdulhameed, S., Ischuk, A., Metzger, S., Kakar, N. (2018): Seismotectonics of the Tajik Basin and Surrounding Mountain Ranges. - *Tectonics*, *37*, 8, pp. 2404—2424.

DOI: http://doi.org/10.1029/2017TC004812

Tectonics

RESEARCH ARTICLE
10.1029/2017TC004812

Key Points:
- A total of 4,500 crustal earthquakes and seismic and geologic stress axes describe deformation in the Tajik basin, Pamir, SW Tian Shan, and Hindu Kush
- N-S compression in the Tian Shan and Pamir and W-E compression in the Tajik basin with partitioning into thrust and strike-slip faulting
- This stress field reflects the combined effects of lithospheric India's northward push and Pamir's gravitational collapse into the basin

Supporting Information:
- Supporting Information S1
- Data Set S1
- Data Set S2
- Data Set S3

Correspondence to:
S.-K. Kufner,
kufner@gfz-potsdam.de

Citation:
Kufner, S.-K., Schurr, B., Ratschbacher, L., Murodkulov, S., Abdulhameed, S., Ischuk, A., et al. (2018). Seismotectonics of the Tajik basin and surrounding mountain ranges. *Tectonics*, *37*, 2404–2424. https://doi.org/10.1029/2017TC004812

Received 14 SEP 2017
Accepted 2 JUL 2018
Accepted article online 8 JUL 2018
Published online 8 AUG 2018

Seismotectonics of the Tajik Basin and Surrounding Mountain Ranges

Sofia-Katerina Kufner[1], Bernd Schurr[1], Lothar Ratschbacher[2], Shohrukh Murodkulov[3], Sanaa Abdulhameed[2], Anatoly Ischuk[3], Sabrina Metzger[1], and Najibullah Kakar[4]

[1]GFZ German Research Centre for Geosciences, Potsdam, Germany, [2]Geologie, TU Bergakademie Freiberg, Freiberg, Germany, [3]Institute of Geology, Earthquake Engineering and Seismology of the Academy Science of the Republic of Tajikistan, Dushanbe, Tajikistan, [4]Norwegian Afghanistan Committee (NAC), Kabul, Afghanistan

Abstract Seismologic and geologic fault-slip data characterize the active deformation of the intramontane Tajik basin and its margins, the Tian Shan, Pamir, and Hindu Kush at the northwestern tip of the India-Asia collision zone. Within this complexly deforming region, the Tajik basin lithosphere forms the backstop for the north-dipping Indian-slab subduction beneath the Hindu Kush but itself delaminates and retreats west and northward beneath the Pamir. Herein, we link crustal deformation to these lithosphere-scale processes, using data from recently deployed seismic networks and geologic observations. Transpressive strike-slip deformation dominates the bounding fault zones along the basin's northern and eastern margins. Seismicity is most intense in the Garm region/Peter I. range of the northeastern basin, where these bounding faults converge and gain a dominant thrust component. Within the basin, seismically and geologically derived *P* axes align with the ~W-trending GPS velocity vectors. Seismicity is concentrated in and at the base of a southward deepening, ~9–15-km-thick wedge. Seismic deformation at the basin's southern margin occurs beneath the Afghan platform, where deep crustal earthquakes likely trace the western end of the Hindu Kush subduction zone. Roughly NNE-striking sinistral strike-slip events outline the Hindu Kush-Pamir transfer system, a zone of distributed shear in the crust overlying the transition of the two oppositely dipping slabs at subcrustal depths. Our observations suggest that crustal deformation in the Pamir and Hindu Kush links with lithosphere-scale processes, whereas deformation in the basin is controlled by the westward gravitational collapse of the Pamir and the resultant basin inversion.

1. Introduction

The intramontane Tajik basin is framed by the Tian Shan to its north and west, the Pamir to its east, and the Hindu Kush to its south (Figure 1a). These mountain ranges have been reactivated with regionally distinct deformation styles in response to the ongoing India-Asia collision. The northward push of India built the northward convex, strongly thickened Pamir orocline (Burtman & Molnar, 1993; Hacker et al., 2017; Mechie et al., 2012), caused lateral extrusion along strike-slip faults in the Hindu Kush (Rutte et al., 2017; Tapponnier et al., 1981), and reactivated the Paleozoic Tian Shan (Avouac et al., 1993; Bande et al., 2017; Käßner et al., 2016). At subcrustal levels, India's indentation into Asia formed a zone of intermediate-depth seismicity (Billington et al., 1977; Fan et al., 1994; Kufner et al., 2017; Pegler & Das, 1998; Sippl et al., 2013). Due to the presence of tomographically imaged high velocity zones at depth, this seismicity has been attributed to ongoing continental subduction/delamination beneath the Hindu Kush and Pamir (Burtman & Molnar, 1993; Koulakov & Sobolev, 2006; Kufner et al., 2016; Schneider et al., 2013; Sippl et al., 2013). In contrast, the Tajik basin's lithosphere between these mountain ranges was proposed to behave as a relatively rigid block (van Hinsbergen et al., 2011). Intense crustal seismicity (Burtman & Molnar, 1993; Fan et al., 1994; Hamburger et al., 1993; Lukk & Yunga, 1988; Nersesov & Popandopulo, 1988), including seven shallow magnitude 7+ earthquakes within the last century, demonstrates the high seismic propensity within the basin and along its margins (Kulikova, 2016, and references therein; Metzger et al., 2017). This poses the question to what extent the crustal seismicity is driven by subcrustal processes.

Due to the intense seismicity, parts of the Tajik basin and Pamir (Garm region/Peter I. range; Figure 1) have been the focus of detailed seismologic studies during Soviet times, resulting in an event catalog spanning ~30 years (CSE catalog; e.g., Nersesov & Popandopulo, 1988; Lukk & Yunga, 1988; Hamburger et al., 1993). Based on these data, continental subduction underneath the Pamir has been proposed (Hamburger et al., 1992). However, these studies concentrated dominantly on the former Soviet part of the collision system.

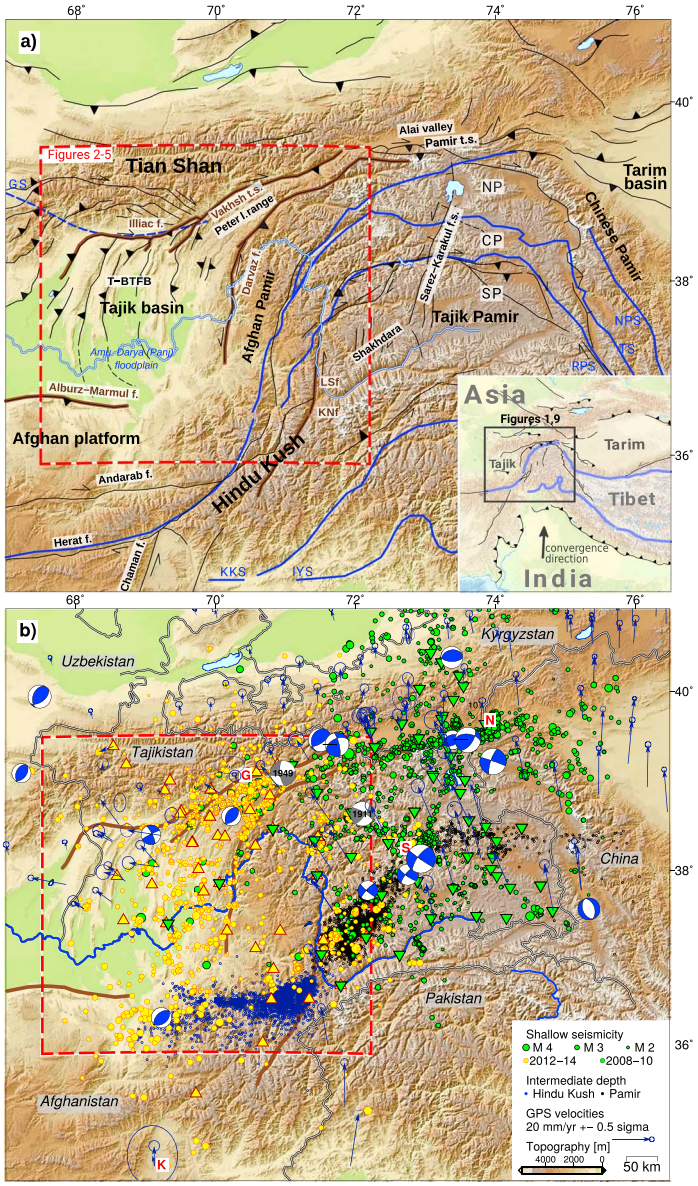

Figure 1. Topographic and seismicity maps of the Hindu Kush-Pamir-Tajik basin collision system. (a) Overview of the tectonic features: faults (black) after Schurr et al. (2014) and this study: KNf = Kapisa-Nuristan fault, LSf = Lake-Shiwa fault, Pamir t.s. = Pamir thrust system, Sarez-Karakul f.s. = Sarez-Karakul fault system, T-BTFB = Tajik basin thrust-fold belt, Vakhsh t.s. = Vakhsh thrust system. The Illiac fault, Alburz-Marmul fault, Vakhsh t.s., Darvaz fault, LSf, and KNf are additionally highlighted in brown and are plotted for reference in Figures 1b to 5. Sutures (bold, blue lines) after Tapponnier et al. (1981), Schwab et al. (2004), Rutte, Ratschbacher, Khan, et al. (2017), and interpreted from Vlasov et al. (1991) and Doebrich et al. (2006) and own work: GS = Gissar, NPS = North Pamir, TS = Tanymas, RPS = Rushan Pshart, KKS = Karakorum-Kohistan-Shyok, IYS = Indus Yarlung. Tectonic units within the Pamir orogen: NP = North Pamir, CP = Central Pamir, SP = South Pamir. Rivers are marked with light blue. Inset shows the location of Figures 1 and 9 in the context of the India-Asia collision zone. (b) Seismicity and GPS rates with respect to stable Eurasia (blue arrows; Mohadjer et al., 2010; Zubovich et al., 2010; Ischuk et al., 2013; Zubovich et al., 2016). Station location (triangles) and shallow (<45 km) seismicity (dots) are color coded by the TIPTIMON (2012–2014) and TIPAGE (2008–2010) projects. TIPAGE seismicity relocated from Sippl, Schurr, Tympel, et al. (2013) and Schurr et al. (2014); TIPTIMON seismicity derived in this study. Intermediate-depth (>100 km) seismicity from Kufner et al. (2017). Blue beach balls represent the double-couple components of all moment tensors from the GEOFON catalog (GEOFON, 2017) from July 2012 to August 2017. Their size is scaled by moment magnitude with minimum and maximum values of 4.2 and 7.2, respectively. Gray mechanisms represent the two largest instrumentally recorded events in the Pamir and along the Tajik basin's margin (Khait, 1949, m_b = 7.6; Sarez, 1911, m_b = 7.3; Kulikova, 2016). Political boundaries are marked with gray lines. Red letters refer to selected cities: G = Garm, K = Kabul, N = Nura, S = Sarez. The dashed red box demarcates the map locations of Figures 2–5.

Therefore, it is still unclear how crustal deformation is linked to the lithosphere-scale processes within the entire Pamir-Hindu Kush-Tajik basin collision system on a regional scale. Herein, we use seismologic methods to assess this question, examining the Cenozoic deformation of the Tajik basin's crust and comparing the seismically constrained deformation field with that inferred from geological data for the last ~10 Myr. Our seismotectonic analysis is primarily based on the recordings of the TIPTIMON seismic network (Schurr et al., 2012, 2013), deployed in the Tajik basin, Hindu Kush, and western Pamir between 2012 and 2014. It continues our recent seismotectonic studies of the Pamir that were based on the earlier (2008–2010) deployed TIPAGE seismic experiment (Schurr et al., 2014; Sippl et al., 2014) and geodetic data (Metzger et al., 2017). Thus, our study combines two large temporal seismic networks, together covering the Tajik basin, Pamir, Tian Shan, and Hindu Kush collision system, placing a high-resolution seismotectonic analysis into a regional tectonic context. In the following, we first focus on the crustal seismic activity within the Tajik basin and its margins, relate it to the late Cenozoic structures and stress field, and then interpret crustal deformation in the framework of the lithosphere-scale processes at the western tip of the India-Asia collision zone.

2. Regional Setting

2.1. Formation History and Cenozoic Structural Map

The Tajik basin is interpreted as a retro-foreland basin with ~7–12 km, ~south- and eastward thickening, Mesozoic-Cenozoic strata (Brookfield & Hashmat, 2001; Burtman & Molnar, 1993; Carrapa et al., 2015; Klocke et al., 2015; Nikolaev, 2002). Basin inversion was inferred to have occurred during the Neogene, forming the Tajik basin thrust-fold belt (Bourgeois et al., 1997; Chapman et al., 2017; Thomas et al., 1994). The inversion may have initiated with weak and localized deformation along the North Pamir margin at ≥20 Ma (Bande et al., 2017; Coutand et al., 2002; Rutte et al., 2017; Sobel & Dumitru, 1997) but intensified later (Cao et al., 2013; Käßner et al., 2016; Sobel et al., 2011; Thompson et al., 2015). Similarly, the first conglomerates shed from the Pamir appear in the upper Oligocene-lower Miocene strata of the (north)eastern Tajik basin. Massive conglomerate deposition and erosion of the incipient folds in the Tajik basin commenced in the middle-late Miocene, highlighted by growth strata (~11 Ma) and angular unconformities (Forsten & Sharapov, 2000; Klocke et al., 2015). The Tajik basin thrust-fold belt seems to be detached along Jurassic evaporites. However, the fact that the leading edge, the western thrust front in the Tian Shan of southeastern Uzbekistan, and the northern lateral margin of the Tajik basin thrust-fold belt, the Tian Shan of northern Tajikistan, involve crystalline basement rocks implies another, deeper detachment below the Jurassic one. The Tajik basin's lithosphere was involved into the late Paleozoic south Tian Shan orogenic belt; this likely includes remnants of the Gissar suture zone underneath the Tajik basin's northern margin (Figure 1a; Brookfield & Hashmat, 2001; Burtman, 1975; Käßner et al., 2017). Studies in the southwestern Tian Shan indicate that it consists of reworked cratonic lithosphere and its cover (Burtman, 1975; Käßner et al., 2017).

We constructed a new structural map of the Tajik basin (Figure 2), by integrating relief (SRTM30), surface, and subsurface structures (interpreted from 1:200,000 geological maps and USSR seismic and drill-hole data [compilation in Gągała, 2014], the Geological and Mineral Resource Map of Afghanistan [Doebrich & Wahl, 2006], satellite images [Google Earth™], and our fieldwork [Gągała, 2014; Käßner et al., 2016]). Internally, the Tajik basin features ~N-NE-trending, westward convex valleys, and ridges; the latter comprise eroded anticlinoria (e.g., Nikolaev, 2002; Thomas, Chauvin, et al., 1994). In the north, these thrusts and folds bend into the ~E-striking Illiac fault zone (*Illiac f.* in Figure 2; Babaev, 1975; Thomas, Chauvin, et al., 1994, Thomas et al., 1994, Thomas et al., 1996). In the south, the Alburz-Marmul fault zone (*Alburz-Marmul f.* in Figure 2), an active transpressional fault zone (e.g., Ruleman et al., 2007), cuts ~NW-trending folds and thrusts that connect—mostly covered by the Amu-Darja River floodplain—with those of the central Tajik basin. The interpretation of basin-wide cross sections (Bourgeois et al., 1997; Chapman et al., 2017; Thomas et al., 1996) indicates that thrust stacking was bivergent, top-to-~E in the western part, and mostly top-to-~W in the eastern part. The Illiac fault zone and the broad belt of dextral transpression in the southwestern Tian Shan and the en-échelon fold-thrusts south of the Amu-Darja River floodplain constitute the northern dextral and the southern sinistral oblique-lateral ramps of the Tajik basin thrust-fold belt, respectively (Figure 2).

2.2. Active Deformation

Deformation in response to the India-Asia collision is ongoing as is evident from GPS-derived displacements and earthquakes (Burtman & Molnar, 1993; Fan et al., 1994; Ischuk et al., 2013; Schurr et al., 2014). The Tajik

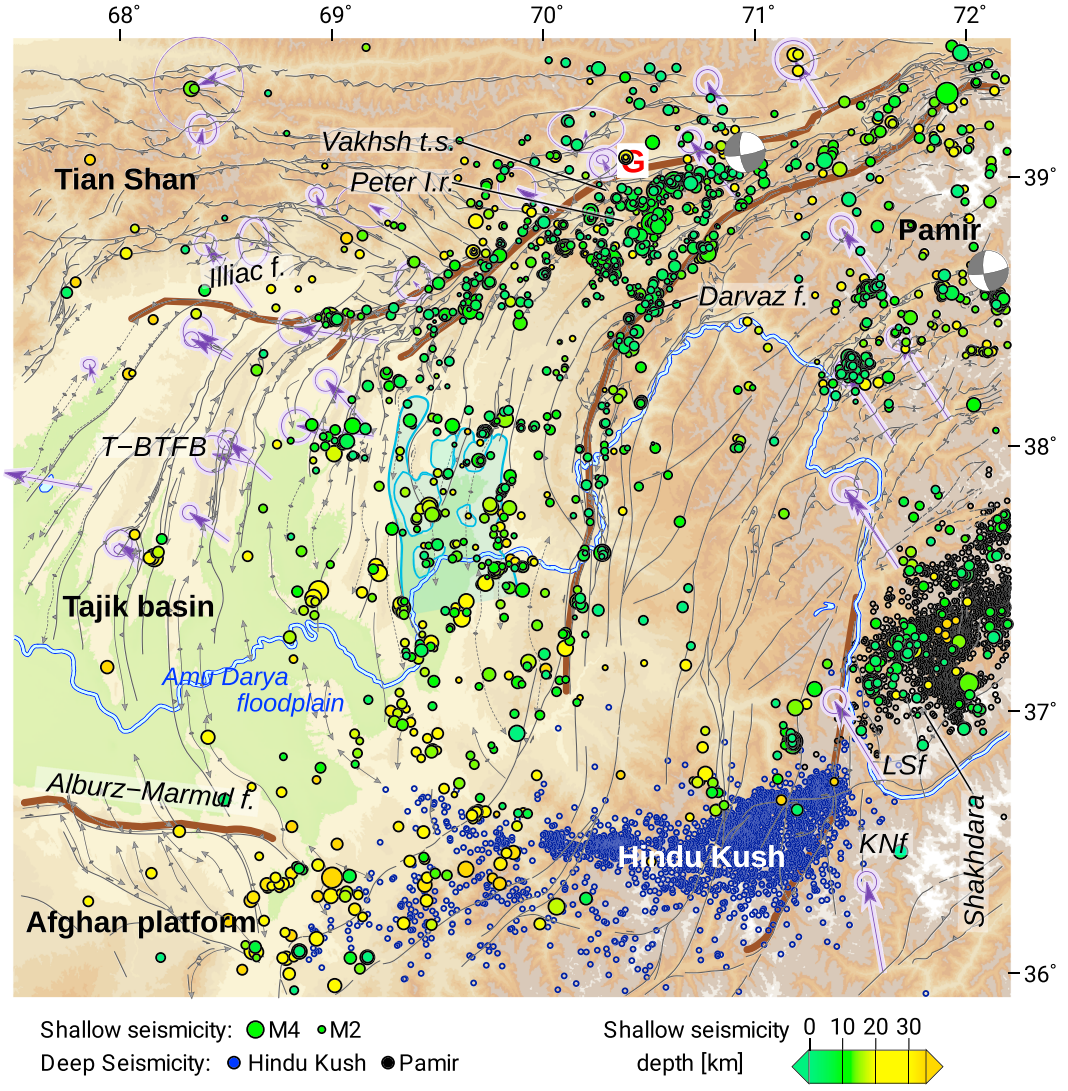

Figure 2. Cenozoic structures in the Tajik basin and surrounding mountain ramps. The map was constructed integrating relief and surface and subsurface structures from field mapping and geologic surveys (see section 2 for references). The structures in the Pamir are from Schurr et al. (2014). The simplified fault traces of the Illiac fault, Alburz-Marmul fault, Vakhsh t.s., Darvaz fault, LSf, and KNf are additionally highlighted in brown as in Figure 1 for orientation. The light blue shaded area in the Tajik basin outlines the area of active salt diapirs. Shallow (<45 km) earthquakes as in Figure 1b but color-coded by depth and scaled by magnitude; deep events (black/dark blue) from Kufner et al. (2017). GPS vectors in purple (see Figure 1 for references and scale). The red "G" indicates the location of the city of Garm. All other features as in Figure 1b.

basin's northern margin defines a broad deformation zone stretching into the southwestern Tian Shan that is bounded in the south by the dextral transpressive Illiac fault zone (Figure 1a). The latter transitions into the Vakhsh thrust system farther east that represents the highly active thrust front of the Pamir with intense seismicity and high shortening rates (Figure 1a) (Käßner et al., 2016; Leith & Simpson, 1986b; Nikolaev, 2002). It links to the Pamir thrust system at the northern front of the Pamir, which features shortening rates of ~13–15 mm/year, accumulating more than a third of the total convergence between India and Asia at this longitude (~34 mm/year; Ischuk et al., 2013; Molnar & Stock, 2009; Schurr et al., 2014; Sippl et al., 2014; Zubovich et al., 2010). The sinistral transpressive Darvaz fault zone (Figure 1a), forming the eastern boundary of Tajik basin over a long distance, was proposed to have accommodated significant northward offset of the Pamir relative to the Tajik basin (Burtman & Molnar, 1993; Nikolaev, 2002), but knowledge regarding its activity is incomplete. Ischuk et al. (2013) derived ~10 mm/year of sinistral shear from GPS measurements, but due to the sparse GPS network, the deformation is poorly localized.

In the south and southeast, the Tajik basin is bounded by the poorly studied Hindu Kush and Pamir of Afghanistan. Transpressive strike-slip faults, like the Albruz-Marmul and the dextral Andarab and Herat, accommodate westward lateral motion of crustal blocks from the Karakorum and Hindu Kush (Figure 1a; Tapponnier et al., 1981; Treloar & Izatt, 1993). These fault zones are bounded in the east by a broad, distributed belt of segmented sinistral strike-slip faults, connecting the Chaman fault of Pakistan and Afghanistan NNE-ward with the Sarez-Karakul fault system in the Central and North Pamir (Figure 1a; Strecker et al., 1995; Schurr et al., 2014; Metzger et al., 2017). Along the Pamir-Hindu Kush transition, these are the sinistral Lake-Shiwa and Kapisa-Nuristan fault systems (Figure 1a). Following these transfer systems into the Pamir, the Pamir's interior was suggested to be segmented along the Sarez-Karakul fault system, with the eastern Pamir moving relatively aseismically northward en bloc, and the western part being seismically more active (Figure 1b; Schurr et al., 2014). Seismic deformation of the western Pamir was explained by the combination of the northward movement of the Pamir and the gravitational collapse and westward lateral extrusion of the Pamir-plateau crust into the Tajik basin, where it causes ~W-E shortening (Schurr et al., 2014; Stübner et al., 2013).

At subcrustal depths, the Pamir and the Hindu Kush are underlain by a curved zone of intense seismicity (Figure 1). Due to the opposite dip of the seismic zones beneath the two mountain ranges, seismicity has been attributed to the ongoing, oppositely inclined continental subduction of Indian and Asian mantle lithosphere (e.g., Burtman & Molnar, 1993; Chatelain et al., 1980; Fan et al., 1994; Negredo et al., 2007; Roecker, 1982). As a competing concept, one slab scenarios were proposed (e.g., Billington et al., 1977; Pavlis & Das, 2000; Pegler & Das, 1998), suggesting that the seismicity is related to a single contorted slab. However, recent seismological studies, based on local earthquake tomography and receiver functions (Schneider et al., 2013; Sippl, Schurr, Yuan, et al., 2013), showed a connection of the Pamir intermediate-depth seismicity with an inferred Moho structure, dipping from the Asian side, clearly favoring a two-slab scenario. In such a two slab scenario, the lithosphere of the Tajik basin would act as a backstop for the north-dipping Hindu Kush subduction zone (Koulakov & Sobolev, 2006; Kufner et al., 2016, 2017; Lister et al., 2008) but at the same time experiencing delamination and rollback beneath the Pamir (Kufner et al., 2016; Schneider et al., 2013; Sippl, Schurr, Tympel, et al., 2013).

3. Methods and Data

3.1. Earthquake Analysis and Location Errors

The earthquake catalog presented here comprises all shallow (<45 km) earthquakes detected using the stations of the TIPTIMON network (Figure 1b; FDSN network codes 6C [2013–2014] and 5C [2012–2014]) and additional permanent stations of the Tajik seismic network and in Kabul (FDSN network codes TJ, IU, and GE; see Kufner et al., 2016, for a detailed description). Additionally, it includes a subset of the TIPAGE catalog (Sippl, Schurr, Tympel, et al., 2013; Schurr et al., 2014; FDSN network codes 7B [2008–2010], 4B [2008–2009], and 6C [2009–2010]) that is derived from stations that were deployed within the Pamir and southwestern Tian Shan. As the TIPTIMON and TIPAGE networks share several stations in the western Pamir (Figures 1b and 3), their configuration allows combining the data sets for a joint analysis.

We obtained earthquake hypocenters by a multistep detection, location, and relocation procedure (Sippl, Schurr, Tympel, et al., 2013). After the initial event association, P and S picks were updated or rejected based on their quality. Earthquakes included from the TIPTIMON deployment time in the final catalog were required to have a root mean square residual smaller than 2 s, at least five P picks and at least one S pick in this initial detection step. We used the regional 1D velocity model of Sippl, Schurr, Tympel, et al. (2013) for the initial event detection and subsequently improved the locations of the joint catalog by event relocation in the regional 3D velocity model of Kufner et al. (2017). Given the highly variable crustal velocity structure in the study region, the relocation in the 3D velocity model was essential for the accurate determination of the event depths. The relative locations were improved by a double-difference relocation scheme. The individual and double-difference event relocation was performed with the software simulps (Eberhart-Phillips, 1993; Evans et al., 1994; Thurber, 1983, 1993) and hypoDD3D (Waldhauser, 2001; Waldhauser & Ellsworth, 2000), respectively. The local magnitudes were calculated from the maximum amplitudes in the waveforms according to Hutton and Boore (1987).

In total, 1,640 shallow earthquakes were detected between July 2012 and April 2014 and jointly relocated with 2,838 events of the TIPAGE catalog, yielding 4,478 events in the final catalog (attached as supporting

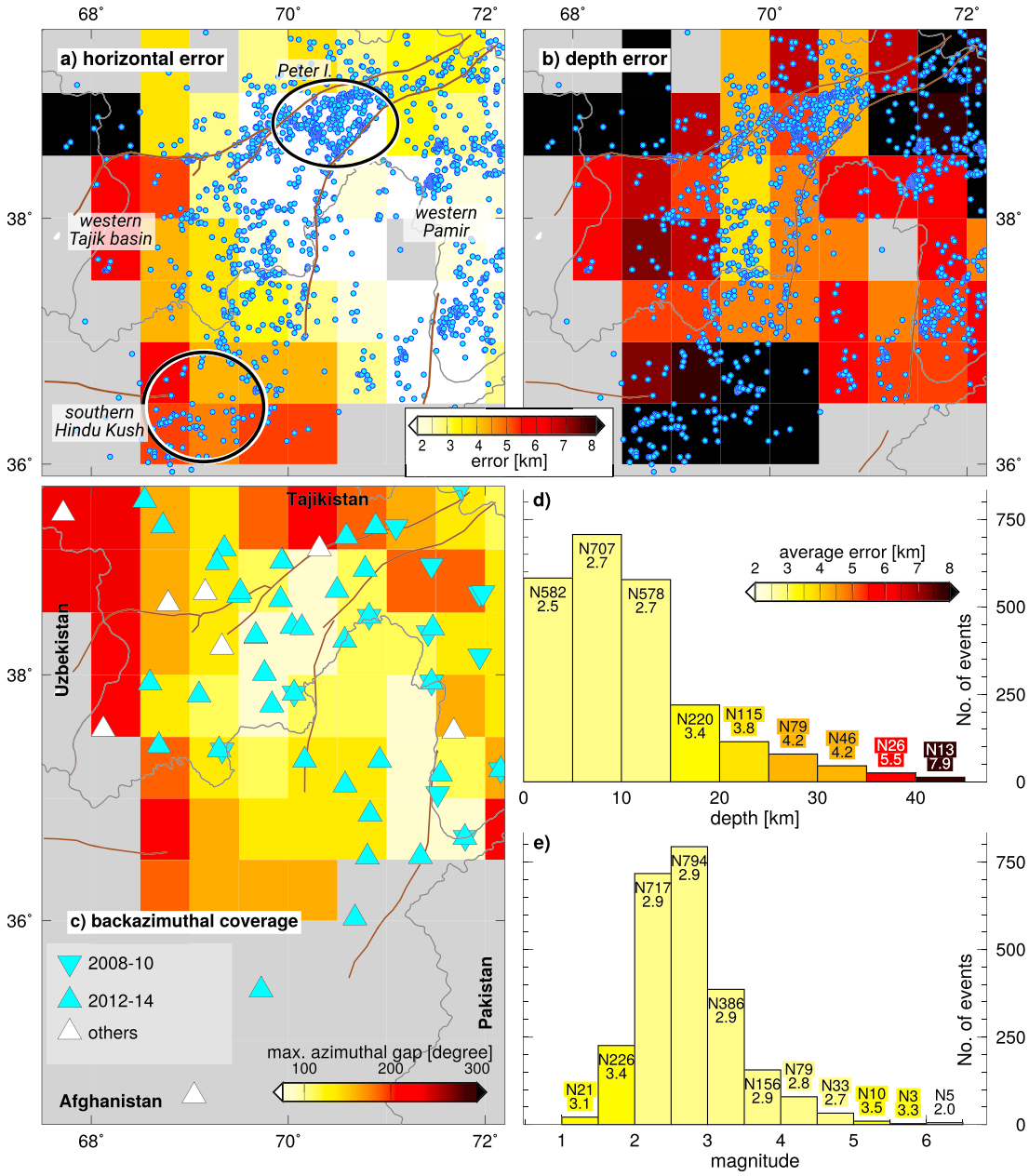

Figure 3. Earthquake location quality. (a and b) Absolute horizontal and vertical location errors. Errors are the axis lengths of the error ellipses in the specific direction from a probabilistic location scheme averaged over all earthquakes in 0.5° × 0.5° bins. The horizontal error is the average over the longitudinal and latitudinal directions. Only bins with at least three events are shown. Political boundaries in dark gray. The simplified fault traces of Illiac fault, Alburz-Marmul fault, Vakhsh t.s., Darvaz fault, LSf, and KNf are highlighted in brown as in Figure 1 for orientation. (c) Station locations and largest azimuthal separation between two stations used to locate a specific earthquake for the events shown in (a) and (b), averaged in 0.5° × 0.5° bins. (d) Depth and (e) magnitude histograms, color-coded by location error. The upper number at the top of each bin refers to the number of events (N), and the lower number is the averaged location error in kilometers (radius of a sphere with the same volume than the error ellipse).

information Data Set S1). The mean root mean square residual of the events in our joint catalog is 0.23 s. The magnitude completeness threshold is approximately at $M_l = 2.4$ (Figure S1), and 76% of all earthquakes were double-difference relocated (Figure S2). The events not relocated with the double-difference scheme were mainly isolated events, which could not be associated with any event cluster (Further discussion on catalog completeness and the data subsets is appended in supporting information Texts S1/S2 and in Figures S1 to S3).

We assessed the location error by calculating probabilistic earthquake locations using the software NonLinLoc (Lomax, 2008). The 68% confidence ellipsoids of the maximum likelihood hypocenters served as the measure for the location uncertainty (Figure 3). The average location uncertainty estimated from the error ellipsoids is ±2.95 km; this value refers to the radius of a sphere with the same volume as the error ellipsoids. In general, the average horizontal errors are smaller than the vertical errors (±2.7 and ± 2.5 km in longitudinal and latitudinal directions versus ±6.2 km in the depth direction). The location uncertainty is smallest in the center of the network (horizontal $<$±2 km; vertical ±3.0–5.5 km; Figures 3a and 3b), as it correlates well with the largest azimuthal gap between the stations used for the location of a specific event (Figure 3c). The regions with the smallest location errors include the Tajik basin, Peter I. range, and western Pamir. East of the Peter I. range, the location quality decreases, probably together with the detection capability. Thus, it is unclear to what extent the decrease in the seismic activity in this region arises from the network-geometry effect. The same concern applies for the western Tajik basin and the southern Hindu Kush, where the vertical location errors are largest (~±10 km). The event-location quality decreases with depth (Figure 3d). However, this trend is biased, as about half of the deepest crustal earthquakes are located in the Hindu Kush, where azimuthal coverage is bad. No correlation occurs between the magnitude and the average location error (Figure 3e). We constrained the relative location errors directly from hypoDD3D, relocating subsets of clusters in the singular value decomposition mode, based on the posterior analysis of the covariance matrix (Waldhauser & Ellsworth, 2000). Compared to the absolute errors, the relative errors are much smaller with an average for all events of ±0.7 km, suggesting that the geometry of the individual seismogenic structures is resolvable in detail.

To assess the dependency of the absolute event locations on the velocity model, we relocated our data set in the 3D velocity model of Sippl, Schurr, Yuan, et al. (2013), which has its highest resolution in the Pamir but also covers the Tajik basin. *P* wave velocities (v_p) of the two models differ by ~0.6 km/s in the Tajik basin sediments (Figure S4a). We find the map view locations of the earthquakes (their longitudinal and latitudinal position) to be mostly independent of the model. However, the event depths can vary by up to 5 km with events locating generally deeper in our model (Figure S4b). The hypocenter depth differences arising from the use of these two models are most pronounced at locations near the transition from the low velocity basin sediments to the high velocity rocks of the Pamir and Hindu Kush. Despite this depth discrepancy, we would argue that the velocity model of Kufner et al. (2017) used herein is currently the most accurate model for the Tajik basin, as the entire basin is located in a well-resolved domain of the inversion (Figure S4b). Nevertheless, it is important to bear in mind that uncertainties stemming from the choice of model may have a severe effect on the event depths, using the available station geometry.

3.2. Seismic Moment Tensors

We derived earthquake-source mechanisms for the strongest events in our catalog from moment tensor inversion (Nábělek & Xia, 1995; Schurr & Nábělek, 1999). Inversions were performed interactively in the time domain, inspecting all data visually and disregarding low signal-to-noise ratio traces. The filter bandwidth was adjusted depending on the size of the event (e.g., between ~10 and 30 s for smaller and 15 and 50 s for larger events). We calculated Green's functions for the 1D velocity model of Kufner et al. (2017), which was derived based on the TIPTIMON data set. The least square inversion for the deviatoric moment tensor was repeated for a suite of trial depths around the hypocentral depth until the solution with the lowest variance was found. This procedure yielded source mechanisms for 81 events, ranging from M_w (moment magnitude) 3.1 to 4.8 (mechanisms attached as supporting information Data Set S2). In addition, we included earthquake-source mechanisms from the TIPAGE deployment (Schurr et al., 2014). These mechanisms were plotted at the updated hypocenter positions (see supporting information Figures S5 and S6 for the components of the two different subsets and data examples).

3.3. Stress Field From Geological Fault-Slip Data

To compare the recent stress-field parameters derived from the earthquake analysis with the long-term evolution of the Tajik basin, we calculated reduced "stress" tensors involving the ratios between and orientations of the principal stresses (e.g., Angelier, 1994), based on mesoscopic fault-slip data collected at 54 sampling locations within our study area. We used the numeric dynamic analysis (Spang, 1972; implemented in the software package of Sperner and Ratschbacher, 1994) for tensor calculation and visualization (Figure S7). Supporting information Data Set S3 gives the sampling locations, the stratigraphic

age of the analyzed rocks, and the calculation parameters. Data Set S3 also includes the published data presented by Thomas, Chauvin, et al. (1994), Sippl et al. (2014), and Käßner et al. (2016). The age of strata involved in the deformation and the available apatite fission-track (U-Th)/He thermochronology (Bande et al., 2017; Chapman et al., 2017; Käßner et al., 2016) indicate that the deformation recorded by these data is younger than middle-late Miocene. Thus, whereas the seismically derived stress directions and the GPS data represent the present deformation regime, the geologic fault-slip data give an average over the past ~15–10 Myr.

4. Results

Seismicity within the Tajik basin and the adjacent mountain ranges is highly partitioned with earthquakes aligning not only along the active faults flanking the Pamir and Tian Shan but also in the basin's interior (Figure 2). Shallow seismicity dominates with ~75% of all hypocenters locating above 12-km depth (Figures 3d and 4). Sparse deeper crustal earthquakes (up to ~35-km depth) occur mainly in the southern part of our study region (southern Tajik basin and Afghan platform). Seismic activity, together with the location accuracy, decreases toward the western Tajik basin at the fringe of the seismic network (Figures 2 and 3). Thus, we will restrict the following presentation of results to the well-resolved domains within our study area (i.e., east of ~68.5°E and north of 36°N). From the basin's margins to its interior and into the adjacent mountains, crustal seismicity is arranged as follows:

Both the northern and eastern margins of the Tajik basin are outlined by localized seismicity: at the eastern margin, seismicity with hypocenters up to 10-km depth coincides with the surface trace of the Darvaz fault zone (Figure 2). Most earthquake-source mechanisms of these events and our only geologic sampling location indicate sinistral strike-slip displacement (Figures 5–7). At the northern margin, seismicity aligns along the Illiac fault zone. East of ~69°E, where our resolution increases, hypocenters form a near-vertical seismically active structure, penetrating to ~15–18-km depth (Figures 5 and 8a) along which our earthquake mechanisms indicate dextral strike-slip displacement. Seismic activity along the Darvaz and the Illiac faults intensifies toward the northeast where both fault zones converge, entering the Garm region/Peter I. range.

Earthquakes within the Garm region/Peter I. range form a triangle of seismic activity in map view (Figure 6), located within a tomographically imaged low-velocity domain (Figure 7). The hypocenters of the northern branch of this triangle vaguely outline a SE-dipping ramp in cross section (Figure 7b), slightly offset south of the surface trace of the Vakhsh thrust, reaching ~12–15-km hypocentral depths. The earthquake mechanisms from events associated with this ramp indicate thrusting with a dextral strike-slip component. The western branch of the triangle of seismic activity is formed by aligned earthquake hypocenters following the trace of the Obikhingou fault (Figure 6). Most of these events are shallower than 10 km, but some sparse deeper events occur as well (down to ~35 km). The southeastern branch of the triangle is formed by the Darvaz fault that changes strike from NNE to NE in the northeastern Pamir (Figure 6). Within this seismically active triangle, we image a fourth zone of activity between the Vakhsh thrust system and the Darvaz fault, which encompasses mostly earthquakes with subhorizontal or subvertical fault planes. Our catalog includes only a few events north of the Garm region/Peter I. range triangle within the high-velocity rocks of the southwestern Tian Shan (Figure 7). Two of these events have thrust-source mechanisms and ~N-trending *P* axes, oblique to the axes of the events aligning close to the Vakhsh thrust system (Figures 6 and 7a). Shallower events in the Tian Shan feature ~NW- and ~NE-striking thrust mechanisms (Figures 6 and 7b).

Southwest of the Garm region/Peter I. range, events in the Tajik basin's interior are sparser and have generally smaller magnitudes (only one of the 18 M_L5+ events of our catalog occurs in the basin). Most of the basin events form a southward deepening wedge with its deepest extent, ranging from ~8–9 km in the north to ~12–15 km in the south (Figure 8). Like the seismicity in the Garm region/Peter I. range, these events roughly coincide with low seismic velocities imaged from seismic tomography. Many rupture mechanisms of events along the base of the wedge have thrust mechanisms with one subhorizontally dipping fault plane (Figures 5–8), similar to those in the central segment of the Garm region/Peter I. range, but with different *P* axis trends. The geologically and seismologically derived *P* axes change from an overall ~NNW–SSE orientation in the Garm region/Peter I. range to ~W-E in the Tajik basin (Figure 4). Seismicity in the basin's interior shallower than the interface at the base of the wedge is sparse and has even smaller magnitudes. Deeper seismicity clusters in a few places. The most intense cluster occurs at the Tajik-Afghan border

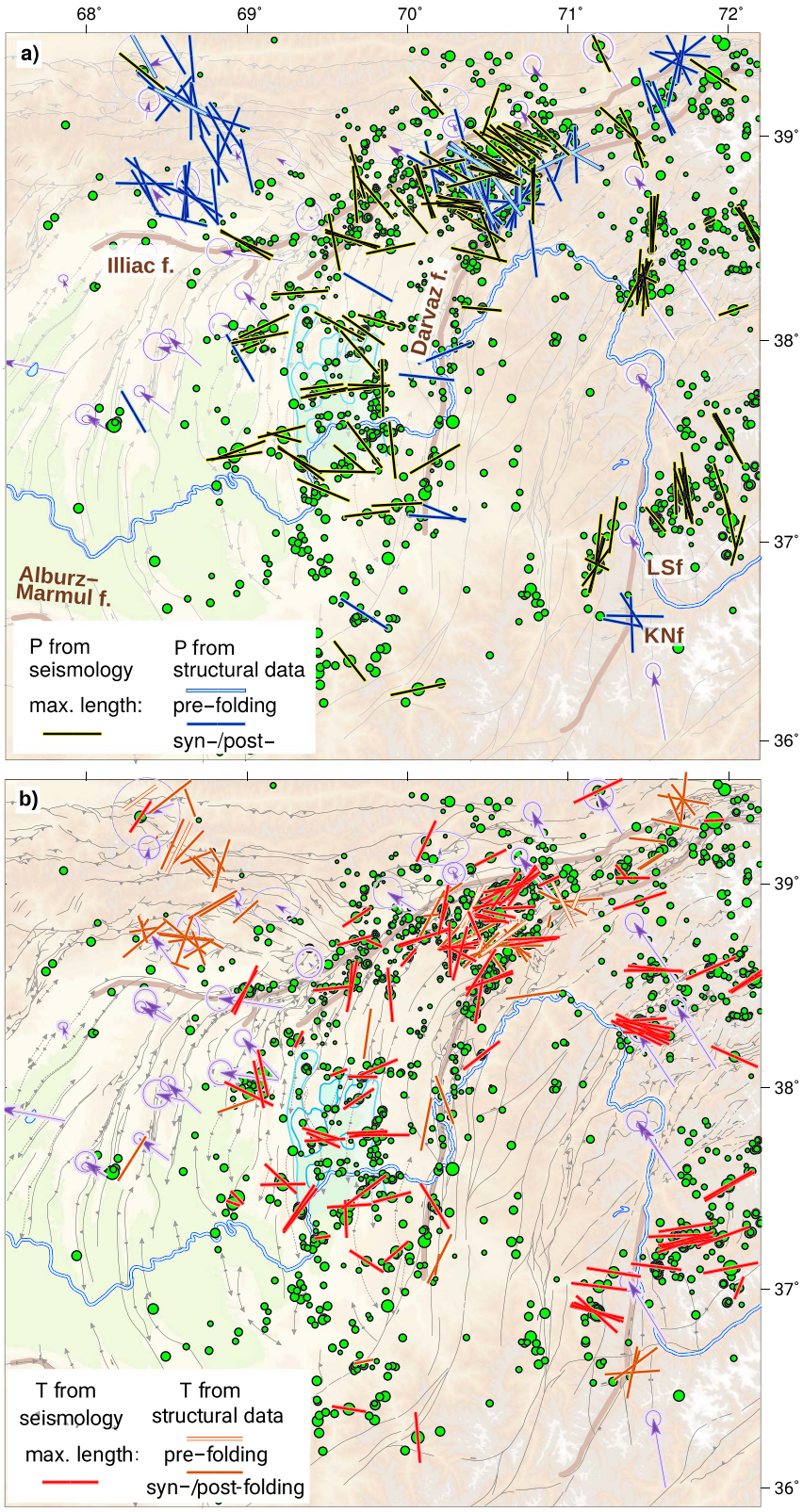

Figure 4. Distribution of seismologic and geologic pressure (P) and tension (T) axes. Pressure (black in (a)) and tension (red in (b)) axes are from seismic moment tensors (associated beach balls plotted in Figure 5). Geologic P (blue in (a)) and T (orange in (b)) axes derived from fault-slip data. Lengths of the axes are normalized to one and projected onto the horizontal map. Shallow seismicity in green. All other features as in Figure 2.

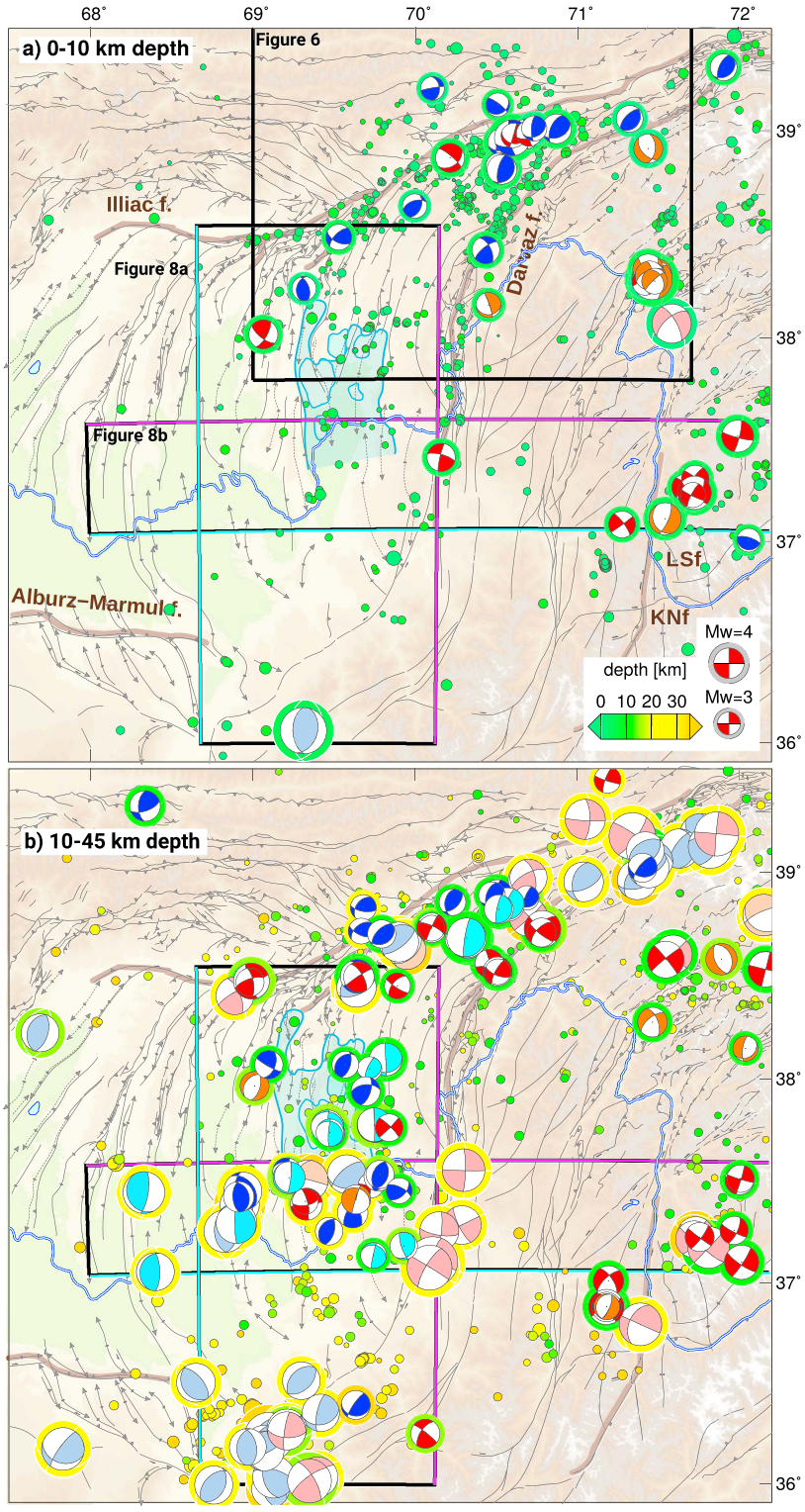

Figure 5. Double-couple component of the moment tensors from this study (bright colors) and from the global CMT database (faded colors) (Dziewoński et al., 1981; Ekström et al., 2012). The mechanisms are colored according to fault type: red, strike-slip; orange, normal; blue, thrust; turquoise, thrusts with one subhorizontal fault plane. The corona of the mechanisms corresponds to their hypocentral depth. Local seismicity and faults as in Figure 2. (a) Events shallower than 10 km. (b) Deeper crustal events (10–45 km depth). Black and blue-pink boxes refer to the map view, respectively, cross-section extent of Figures 6, 8a, and 8b. The blue lines indicate minimal and the pink lines maximal profile normal distance in the Figures 8a and 8b.

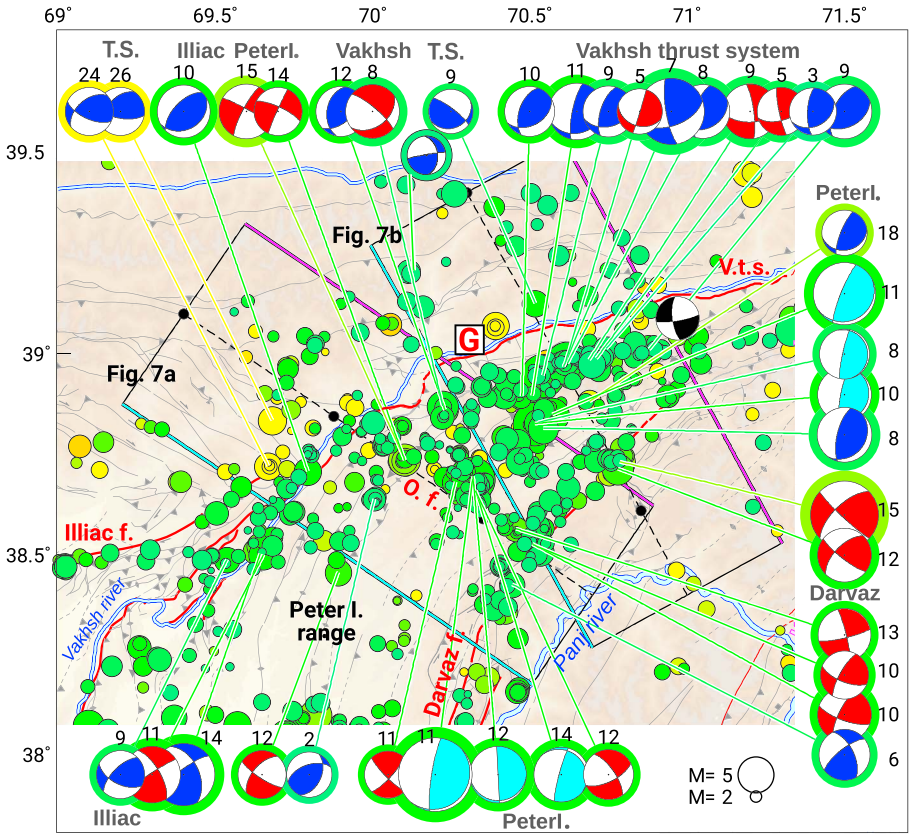

Figure 6. Zoom into the Garm region/Peter I. range (Figure 5 for map location). Color-coding of seismicity with depth as in Figure 4. The number on top of the associated beach balls and the surrounding colored circle indicate the hypocentral depth. The color of the mechanisms indicates the fault type (see annotation in Figure 5). The black mechanism is the focal mechanisms for the 1949 Khait earthquake (m_b 7.6; Kulikova, 2016). Major active faults, as determined from fieldwork, are in red (V.t.s. = Vakhsh thrust system, O.f. = Obikhingou fault). Boxes indicate the section lines shown in Figures 7a and 7b. Dots along the central black line are 50-km marks. The blue line indicates minimal, the pink line maximal profile normal distance (in accordance to the color-scaling of the earthquakes in Figure 7). The red "G" indicates the location of the city of Garm.

(~69.5°E/37.5°N) and features thrust but also dextral strike-slip mechanisms (Figure 5). At the transition of the Tajik basin to the Afghan platform, seismicity is not focused along one active fault zone, as it is at the basin's northern and eastern margins. Instead, we image a diffuse, ~E-trending belt of earthquakes beneath the Afghan platform east of the surface trace of the Alburz-Marmul fault zone and west of the intermediate-depth Hindu Kush earthquake cluster (Figures 2 and 5). Hypocenters of the crustal events beneath the Afghan platform penetrate as deep as 40 km (Figures 2–5) and occur in higher velocity material than those clustering in the Tajik basin (Figure S4). We only could determine one NNE-striking thrust mechanism from these earthquakes, but global CMT-catalog mechanisms indicate ~N-, NE-, and NW-striking thrust events and isolated strike-slip earthquakes (Figure 5b). The crust above the prominent intermediate-depth Hindu Kush earthquake zone is almost completely aseismic (Figures 2–5 and 8), but shallow seismicity resumes NE of the Hindu Kush intermediate-depth earthquake cluster and east of the Lake-Shiwa and Kapisa-Nuristan faults in the Shakhdara region of the southwestern Pamir (Figures 2 and 8b). Earthquakes NE of the Hindu Kush intermediate-depth earthquake cluster have mainly strike-slip mechanisms, which are also the dominant mechanisms for events in the Shakhdara region.

5. Interpretation and Discussion

Two major processes likely control the current deformation of the Tajik basin, Pamir, and Hindu Kush. (1) The northward motion of Indian lithosphere beneath the Hindu Kush and the Pamir (e.g., Kufner et al., 2016; Metzger et al., 2017; Sippl, Schurr, Yuan, et al., 2013) and (2) the gravitational collapse and lateral extrusion of the thickened and elevated Pamir-plateau crust into the depression of the Tajik basin (e.g., Käßner et al.,

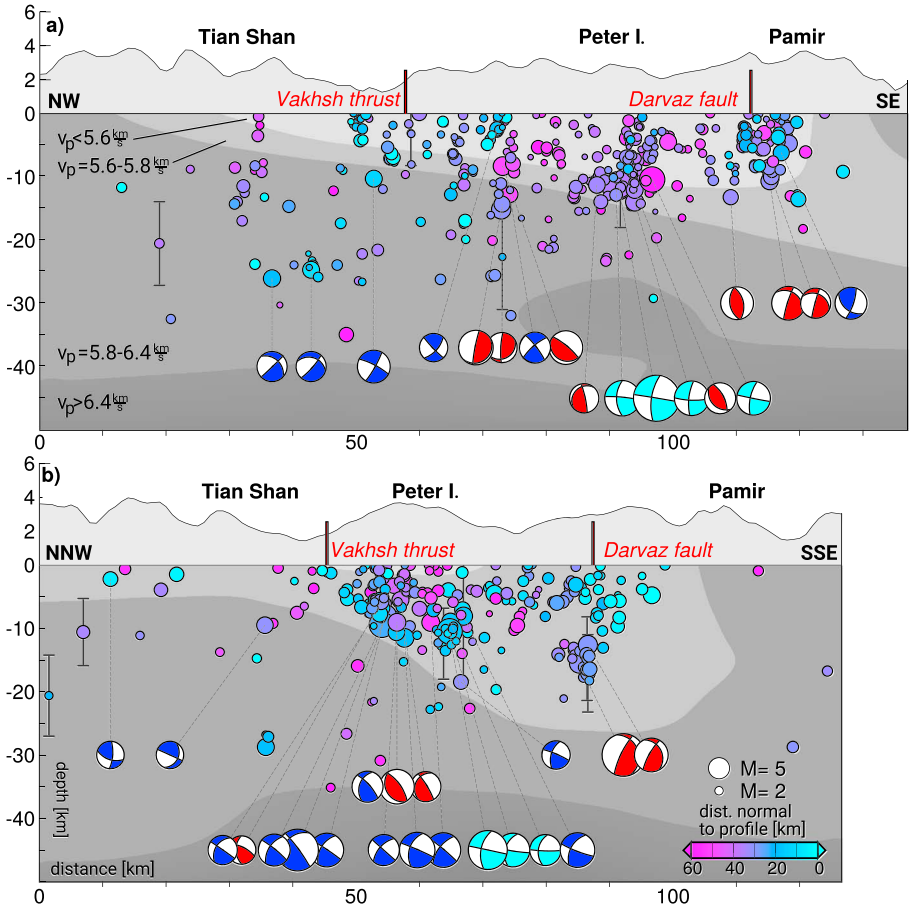

Figure 7. Vertical sections through the Garm region/Peter I. range seismicity (Figure 6 for section lines). Focal mechanisms are rotated in the cross section and represent back projections, as seen from a viewpoint orthogonal to the profile. Color-coding of the earthquakes indicates their profile-normal distance. Events with average location error larger than 5 km are plotted with error bars. The background map shows the *P* wave velocity model of Kufner et al. (2017), which was also used to relocate the earthquakes, along the center trace of the sections. Gray domain on top of the profiles is the projected topography.

2016; Rutte, Ratschbacher, Khan, et al., 2017; Schurr et al., 2014; Stübner et al., 2013). The stress axes from this study, covering a few years (earthquake-focal mechanism) and a ~10-Ma period (geologic fault-slip analysis), show the same orientation variation on a regional scale and allow to resolve the interconnection of the different tectonic elements involved in the collision.

5.1. W-E Shortening in the Tajik Basin's Interior

For most events in the Tajik basin for which we could estimate focal mechanisms, the *P* axes are parallel to the ~W trend of the GPS-velocity vectors. Additionally, often one of the two possible fault planes aligns subhorizontally. Schurr et al. (2014) interpreted this configuration as reflecting shortening of the Tajik basin strata due to gravitational collapse of the Pamir-plateau crust into the depression occupied by the basin. They suggested slip along a basal décollement, marked by the Jurassic evaporite layer, to explain the earthquakes with subhorizontally orientated thrust mechanisms in their data set. Because deformation in salt is normally ductile, earthquakes would then occur where the salt layer is thinned or has pinched out. In our catalog, the most intense seismicity along the base of the wedge occurs north of the Panj river, in an area of active salt diapirism, where the diapirism may have deprived the décollement of salt (Leith & Simpson, 1986a; Figures 2, 4, and 5). Thus, this configuration supports the hypothesis of earthquake clustering along the evaporite décollement. However, with hypocenter depths from ~9 km in the northern to ~15 km in the southern Tajik basin, a significant number of earthquakes are deeper than the evaporite décollement at 7–12 km, whose depth was approximated by geologic and drilling data (Brookfield & Hashmat, 2001;

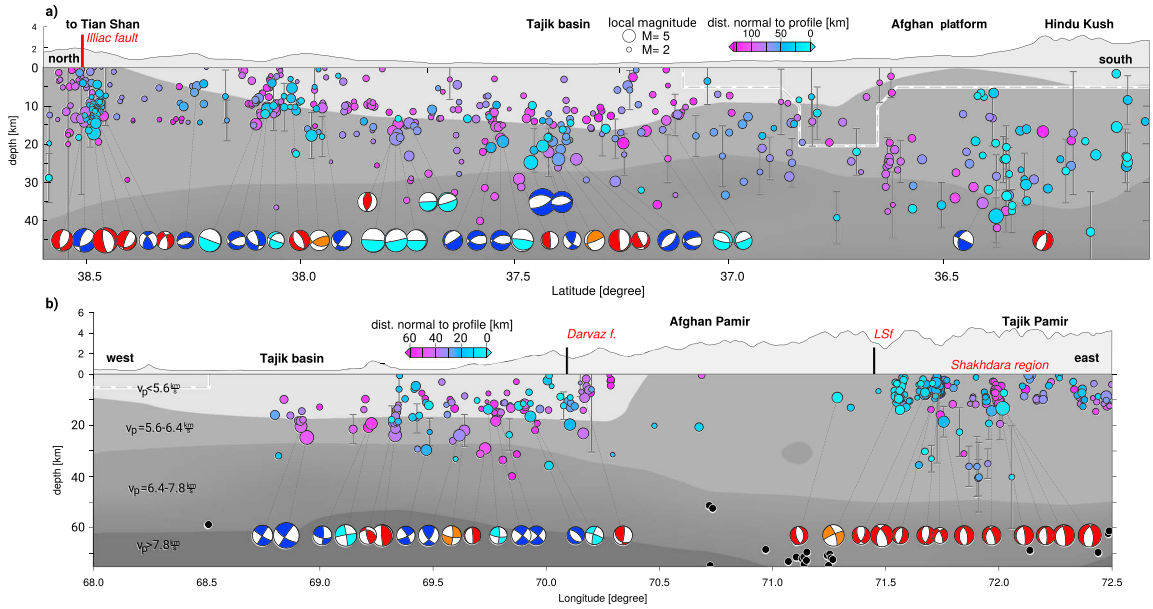

Figure 8. Depth sections through the Tajik basin (Figure 5 for section lines). Color coding and rotation of the focal mechanisms as in Figure 7. Dashed white line encloses low resolution of the velocity model. (a) N-S profile; (b) W-E profile. LSf = Lake-Shiwa fault. In the velocity model, the v_p = 7.8 km/s contour approximately denotes the crust-mantle boundary. Black circles are the shallowest earthquakes associated with the Pamir intermediate depth seismicity.

Nikolaev, 2002). This discrepancy could be due to either an imprecisely determined evaporite décollement depth or a systematic shift of our earthquake hypocenters (e.g., up to 5 km model error for events in the basin; Figure S4). Alternatively, the events could indicate sliding along a deeper décollement, possibly along the sediment-basement contact, which would be in accordance with a southward thickening of sediments in the Tajik basin (Brookfield & Hashmat, 2001; Nikolaev, 2002). Interestingly, events in the central Tajik basin (e.g., at ~38°N), although numerous, have dominantly small magnitudes (<4.5; see Figure S3b). Accordingly, this region appears nearly aseismic in global catalogs (e.g., USGS (USGS, 2017), EHB (Engdahl et al., 1998) or ISC (International Seismological Centre, 2014); Figure S3) that cover larger timespans (~40 years) but have larger completeness magnitudes (~4.5) than our data set. These generally smaller earthquakes in the basin's interior might indicate that only small patches along the basal décollement and not the entire length of the décollement ruptured during one seismic event.

From the earthquake data alone, we cannot exclude the possibility that the subvertical fault plane and not the subhorizontal one is the rupture plane. In this case, the mechanisms would indicate dominantly thrusting along near-vertical faults within the Tajik basin. However, given the overall E-W directed compressional tectonics of the basin, W-pointing GPS-velocity vectors, the alignment of earthquake hypocenters along an approximately horizontal structure, which follows a single contour of the *P* wave velocity model (v_p = 5.6 km/s; Figure 8), vertical faulting seems less likely. Thus, we suggest that thin-skinned E-W shortening, possibly driven by the push of the collapsing Pamir plateau, controls seismic deformation in the basin (Schurr et al., 2014). At least for the last ~40 years, the events in the central Tajik basin seem to be characterized by smaller magnitudes. This is in contrast to the basin's margins, where the historically largest earthquakes were located (Kulikova et al., 2016). The few deeper earthquakes beneath the Tajik basin would consequently have to be associated with deformation in the basement. Such seismicity could be triggered by the response of the basin's basement to delamination and rollback of lower crust and lithospheric mantle beneath the Pamir (Sippl, Schurr, Yuan, et al., 2013). Hamburger et al. (1992) proposed a similar reason for events deeper than ~15 km in the Garm region/Peter I. range.

Existing geologic data indicate that the seismically active portion of both the Darvaz and the Illiac fault zones penetrates into the basement below the evaporite décollement (Bourgeois et al., 1997; Thomas et al., 1996). For the Illiac fault zone, our earthquake data confirm this interpretation, as seismicity associated with the surface trace of this fault penetrates as deep as ~15–20 km, which is deeper than the proposed sediment thinness (Brookfield & Hashmat, 2001; Nikolaev, 2002). For the Darvaz fault, the situation is less clear as its

seismogenic depth in the central segment is ~10 km. Nevertheless, the sinistral strike-slip displacement inferred from seismicity and fault-slip field data is in accordance with the sinistral shear inferred from geologic and GPS observations (Ischuk et al., 2013; Kuchai & Trifonov, 1977; Trifonov, 1978). Whereas the GPS measurements are too sparse to assess where deformation is localized, the aligned seismicity imaged herein suggests confined deformation. Furthermore, from the absence of thrust events, we infer that thrusting between the Pamir and the Tajik basin along the Darvaz fault zone is inactive or aseismic today. This is in accordance with the neotectonic field mapping (Trifonov, 1978).

5.2. Thrusting and Lateral Extrusion Within the Garm Region/Peter I. Range

Our results on seismicity and earthquake-rupture mechanisms within the Garm region/Peter I. range confirm the seismicity pattern obtained from the local, Soviet-time seismologic studies (Soviet/US-CSE earthquake catalog; Nersesov & Popandopulo, 1988; Lukk & Yunga, 1988; Hamburger et al., 1993). Both catalogs show a similar segmentation into seismically active regions: Earthquakes are mostly shallower than ~12 km, split into individual segments, and separated by the Obikhingou fault from the seismically less active Tajik basin (Figure S8). However, due to the use of well-timed digital data, a 3D velocity model, and double-difference relocation, the events in our catalog outline the geologic structures more sharply (e.g., the seismic structure associated with the Vakhsh thrust; Figure 7a). The strain pattern derived from the CSE focal mechanism analysis (Lukk et al., 1995) is in accordance with the overall NNE-SSE compression resolved in our study. Thus, the good agreement of seismogenic features presented in these two independent data sets indicates their accuracy and consistency through time.

The seismically active domain of the Garm region/Peter I. range coincides with low v_p imaged by local tomography (Kufner et al., 2017). As sediments are characterized by lower seismic velocities than basement rocks, the low v_p domain likely maps the Tajik basin sediments imbricated between the crystalline basement rocks of the Pamir and Tian Shan, a configuration also proposed from field mapping (Burtman & Molnar, 1993; Hamburger et al., 1992). The SE-dipping seismic ramp, forming the northern termination of the intense seismicity of the Garm region/Peter I. range, collocates well with the northern *P* wave velocity contrast (Figure 7). This suggests an alignment of the northern branch of seismicity along an interface between the Tajik basin sediments (low v_p) and the Tian Shan basement rocks (high v_p). Dependent on the velocity model used for earthquake location, this interface would reach depths from ~7 up to 12 km (see model-dependent depth variation in Figure S4). As the surface trace of the Vakhsh thrust zone is located directly updip of the seismically active zone at depth, these events likely indicate oblique thrusting on the Vakhsh thrust. If this is the case, the decrease in seismicity shallower than 5-km depth might indicate that the upper part of the Vakhsh thrust is either creeping or locked. Recent GPS measurements show a large surface velocity contrast across the fault (Metzger et al., 2018). This could indicate a creeping behavior along of the fault's shallowest segment. During our observation period, the seismogenic interface likely associated with the Vakhsh thrust hosted the largest crustal earthquakes. Thus, we propose that it accommodates most of the today's northwesterly motion of the Pamir, both in shortening and dextral shear (Lukk et al., 1995, 2008). The events with subhorizontal fault planes in the center of the Peter I. range could then indicate sliding along a basal décollement either at the base of the sediments or in the basement rocks (e.g., Hamburger et al., 1992; Lukk et al., 1995). Alternatively, they might indicate shortening along steeply dipping backthrusts, if the more vertical focal plane is the rupture plane (e.g., Leith & Simpson, 1986b; Pavlis et al., 1997).

The events located in the basement rocks of the Tian Shan likely indicate shortening as well, expressed through the reactivation of E- to SE-trending Paleozoic basement structures. Sippl et al. (2014) observed such a structural control in the aftershock sequence of the 2008 M_w 6.6 Nura earthquake along the eastern continuation of the Vakhsh thrust system. The 1949 m_b 7.6 Khait earthquake (Evans et al., 2009) at the northeastern termination of the Garm region/Peter I. range could also belong to the group of basement earthquakes in the Tian Shan. The event locates close to the leading edge of the Vakhsh thrust system (Figure 6). Macroseismic observations, however, place it into the Tian Shan (Bindi et al., 2014). One of its nodal planes parallels the Vakhsh thrust but has sinistral strike-slip kinematics. The other nodal plane strikes ~NNE, subparallel to faults in the Garm crystalline-basement complex in the Tian Shan to the north and possible kinematically related faults in the Vakhsh thrust system.

Summarizing, we attribute the intensity and the complexity in the distribution of seismicity in the Garm region/Peter I. range to three interconnected aspects of the current deformation field. (1) The Garm

region/Peter I. range occupies the northeastern edge of the Pamir orocline, where northward translation of the Pamir along the Darvaz fault zone and the western Pamir interacts with focused thrusting along the northern Pamir front (Vakhsh thrust system). (2) The Garm region/Peter I. range accommodates a significant portion of the dextral displacement along the northern margin of the lateral extrusion zone, where Pamir-plateau crust is moving westward into the Tajik basin proper. (3) The Garm region/Peter I. range likely is strongly influenced by the heterogeneity of the underlying Tian Shan basement structure, for example, inherited normal and strike-slip faults (Figure 2; Hamburger et al., 1992).

5.3. Focused Crustal Deformation in Afghanistan

The depths of earthquakes located underneath the Afghan platform are less well constrained than the basin events. However, the horizontal locations of the crustal earthquakes in Afghanistan are still relatively accurate (Figure 3), allowing a discussion on the epicentral distribution of these events. The crustal earthquakes beneath the Afghan platform cluster at the western termination of the intermediate-depth Hindu Kush seismicity, which was proposed to be driven by ongoing slab break-off (Kufner et al., 2017; Lister et al., 2008). Numerical modeling showed that slab detachment, that is, the loss of the gravitational slab pull force, can cause uplift in the crust above (e.g., van Hunen & Allen, 2011). This uplift might be relatively coherent over a large region, causing deformation to focus along its margins. Thus, we propose that the crustal earthquakes at the western edge of the Hindu Kush intermediate-depth seismicity and the absence of crustal seismicity directly above the nest of deep seismicity might be the expression of such a phenomenon. Alternatively, crustal earthquakes within the central Hindu Kush could happen with larger intervals than our observation time, but also exceeding the observation time of global catalogs (Figure S3).

5.4. Crustal Deformation Related to Mantle Processes

On a regional scale, our data suggest the existence of two sinistral transfer corridors for deformation with focused crustal seismicity at their northern tips and subdued seismicity east of them (labeled "1" and "2" in Figure 9). (1) The Sarez-Karakul fault system with the eastern Alai valley seismic cluster at its northern tip and the relatively aseismic eastern Pamir in the east. The Sarez-Karakul fault system hosted magnitude 7+ strike-slip earthquakes in 1911 and 2015 (Sarez earthquakes; Ambraseys & Bilham, 2012; Kulikova et al., 2016; Sangha et al., 2017, Metzger et al., 2017). Three 6+ thrust earthquakes occurred at its northern tip (1974 Markansu; Ni, 1978; Jackson et al., 1979; Sippl et al., 2014; 2008 Nura, Teshebaeva et al., 2014; Sippl et al., 2014; 2016 Sary Tash). (2) The Darvaz fault zone of the easternmost Tajik basin with the Garm region/Peter I. range seismic cluster in the north and the mostly aseismic Afghan Pamir in the east. The Darvaz fault zone hosted the 1949 7+ Khait earthquake at its northern tip.

The formation of these transfer corridors might be driven by subcrustal processes. We (Kufner et al., 2016) proposed that the two oppositely dipping zones of intermediate-depth seismicity beneath the Pamir and Hindu Kush trace Indian and Asian lithospheres. In this model, the northward advancing cratonic Indian lithosphere (Cratonic India) forces the north- and westward delamination and rollback of the Asian lithosphere beneath the Pamir. At the same time, India's thinned western margin (Marginal India) first underthrusts alongside Cratonic India and then separates and subducts beneath the Hindu Kush (schematically shown in Figure 9). Based on the study of crustal seismicity presented here, we speculate that the proposed subcrustal lithospheric boundaries determine the deformation in the crust and locate the transfer corridors identified above. (1) In the southwestern Pamir, the ~NE-trending belt of shallow crustal earthquakes is congruent with the ~NE-trending zone of intermediate-depth seismicity (Figure 9a) that is likely tracing the western edge of Cratonic India at mantle depth. Nodal planes and slip vectors of the crustal earthquakes also follow this ~NE trend (Figures 4 and 5). The overall strike-slip and more rarely normal mechanisms suggest that seismic deformation occurs along a network of interconnected faults. The seismicity, however, does not clearly coincide with distinct surface structures. We interpret this distributed shear zone as the shallow and early-stage manifestation of the India-Asia plate boundary at mantle depth. It is accommodating displacement between the Asian crust carried on top of Indian lithosphere northward and the more stationary Asian crust and mantle farther west. Thus, the presence of a shear zone with earthquake-source mechanisms indicating relative displacement between a western (Hindu Kush) and an eastern (Pamir) unit supports a two-slab scenario for the explanation of the zone of intermediate-depth seismicity underlying these mountain ranges. This shear zone may also transfer deformation from the sinistral strike-slip faults of Afghanistan and Pakistan in a right-stepping array toward northeast, connecting them to

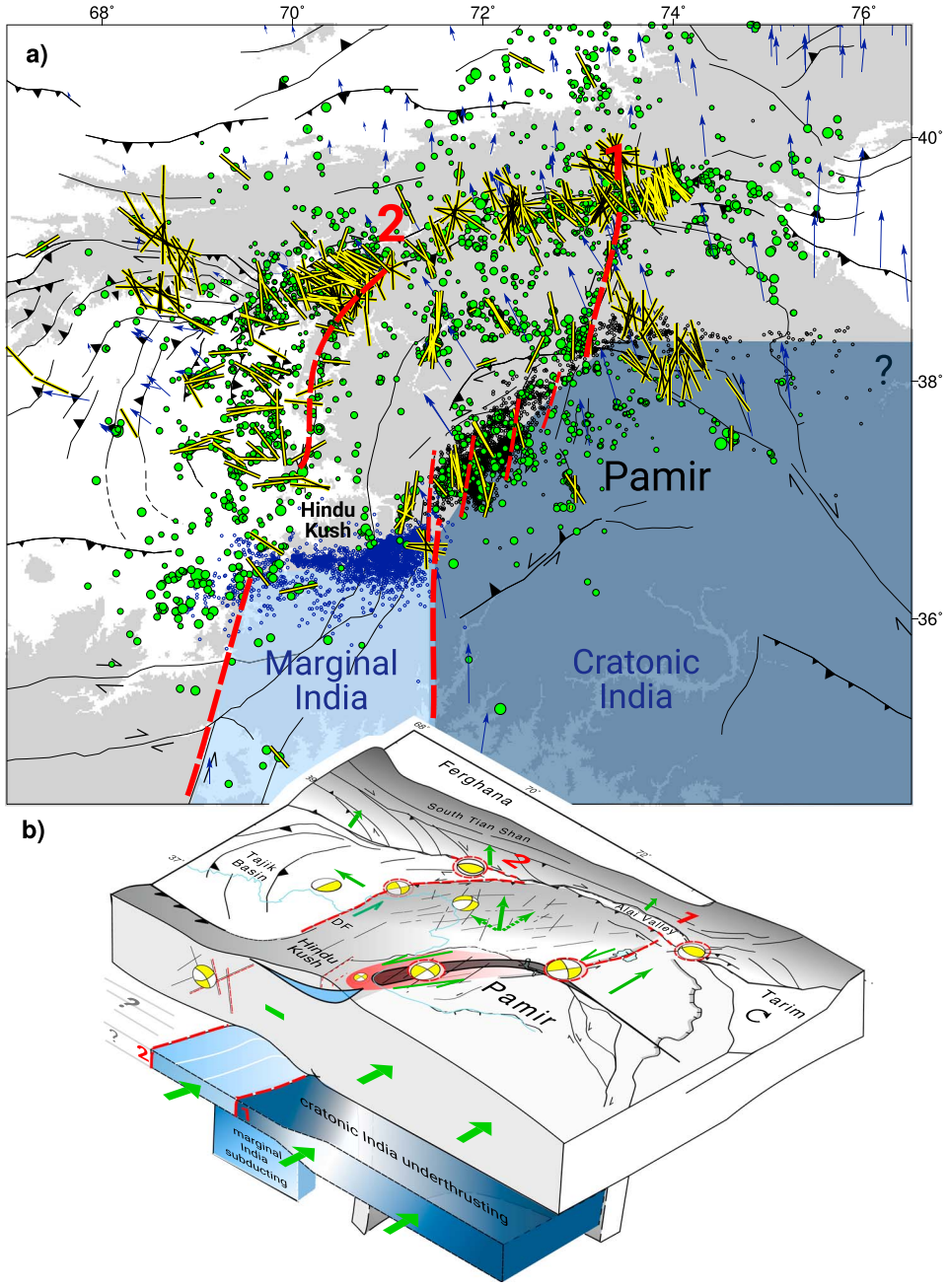

Figure 9. Tajik basin seismicity and neotectonics at the western edge of the India-Asia collision zone. (a) Seismicity catalog and stress orientations from earthquake-focal mechanisms (yellow on black) and from fault-slip data, representing the stress field over the last ~10 Ma (black on yellow). Crustal earthquakes in green, intermediate-depth seismicity in black (Pamir) and blue (Hindu Kush), and GPS velocity vectors in blue. See Figure 1 for references. The gray domain represents topography higher than 2,000 m. The red dashed lines (labels "1" and "2") indicate two crustal transfer corridors that we suggest to align with the subcrustal boundaries of Marginal and Cratonic India farther south (see section 5.4 for a detailed discussion). South of ~37°E, the dashed red lines and the blue outlines mark the map view extension of Marginal and Cratonic Indian lithosphere according to the interpretation of Kufner et al. (2016). (b) Interpretation of the neotectonics. The sketch shows Indian lithosphere at subcrustal depths as light and dark blue bodies (crustal and lithospheric thickness not to scale); the red dashed lines mark the outline of the transfer corridors according to section 5.4. Yellow focal mechanisms indicate the style of dominant crustal deformation. Green arrows show directions of material flow within the crust imposed by the Indian convergence at subcrustal depths (dominantly for Pamir and Hindu Kush) and the gravitational collapse of the western Pamir (dominant for the Tajik basin). Sketch and kinematics in the central/eastern Pamir and in the Tian Shan are adopted from Schurr et al. (2014) and Käßner et al. (2016), respectively.

the Sarez-Karakul fault system (Metzger et al., 2017; Rutte, Ratschbacher, Khan, et al., 2017; Schurr et al., 2014; Stübner et al., 2013). The Sarez-Karakul fault system then seems to act as a transfer corridor for deformation through the Pamir. (2) The Hindu Kush continental subduction zone may still transmit stress to the Tajik basin lithosphere, building up the second transfer corridor along the Darvaz fault, as the strike-slip movement along the fault is still active.

We suggested that lateral extrusion of Pamir rocks is responsible for the high seismic activity and frequent large earthquakes in the Garm region/Peter I. range. However, given the complex crustal and mantle structure and the near-syntaxis location of the Pamir-Hindu Kush-Tajik basin, other tectonic processes might contribute to the observed strong and complex deformation field. Ideas suggested for surface-crust-mantle coupling at plate-boundary syntaxes (e.g., western and eastern Himalayan syntaxes, Alaska, Caucasus, etc.) might be applicable for our study region as well. Based on geodetic, modeling, and field studies, it has been shown that oblique convergence can cause orogen parallel material flow throughout the crust and upper mantle as well as the rotation of surface velocity vectors, surface strain, and fault orientations (Finzel et al., 2015; Hu et al., 2012; Sternai et al., 2016; Whipp et al., 2014). Such processes might also contribute to the radial strain field we observe in the Tajik basin. Erosion and exhumation may also have an effect on strain localization in the crust (Enkelmann et al., 2015; Wang et al., 2014; Zeitler et al., 2015), which might play a role at the orographic transition from the Tajik basin to Pamir and Hindu Kush mountains.

6. Conclusions

Based on 4 years of temporarily deployed seismic networks, we derived an earthquake and source-mechanism catalog for the crustal seismicity within the Tajik basin and the adjacent Pamir, Hindu Kush, and Tian Shan. We interpret the seismic features together with the long-term stress field derived from geologic fault-slip data, an updated Cenozoic fault map, and in relation to the subcrustal processes beneath the Hindu Kush and Pamir. Our results suggest that the regional seismic deformation can be characterized by three domains with different activity:

1. We find that earthquakes that occur on active faults bounding the basin (Illiac and Darvaz fault zones) are predominantly strike-slip. In the northeastern Tajik basin, where the Pamir and Tian Shan converge (Garm region/Peter I. range), strike-slip earthquakes associated with the dextral Illiac and sinistral Darvaz fault zones transition into a zone of oblique thrusting. The Garm region/Peter I. range hosts not only the largest instrumentally recorded earthquakes along the basin's margins (Kulikova, 2016, and references therein) but also exhibits the most frequent crustal seismicity in our catalog. We suggest that this intense seismicity occurs in response to the combined effects of the northward pushing Indian indenter and the westward extruding Pamir-plateau rocks into the Tajik basin.
2. Hypocenters in the Tajik basin gradually deepen southward from 9 to 15 km, possibly outlining the Jurassic evaporite décollement or a deeper detachment. The stress orientations derived from seismic moment tensors match with the trends of the westward-oriented GPS-velocity vectors. We find that this pattern is consistent with a model of gravitational driven extrusion of Pamir crust onto the Tajik basin. Other processes associated with the near syntaxis-location of the study region might affect tectonics as well.
3. Crustal seismicity in northeastern Afghanistan appears to be dominated by compression at the western edge of the Hindu Kush continental subduction zone. The Afghan Pamir north of the Hindu Kush subduction zone exhibits little seismicity, moving north- and westward with little internal deformation. Farther east, a domain of interconnected strike-slip faults in the Hindu Kush and southwestern Pamir outlines a transfer zone. We suggest that this transfer zone is accommodating the relative movement between the two segments of the horizontally tearing Indian lithosphere at subcrustal levels (Cratonic and Marginal India in Figure 9). This implies that subcrustal lithospheric boundaries can be traced as complexly deforming regions in the overlying continental crust.

Acknowledgments
This research was funded as part of the CAME project bundle TIPTIMON (funded by the German Federal Ministry of Education and Research; support codes 03G0809 and 3G0878B), the DFG bundle TIPAGE (PAK 443), and the GFZ via its expedition funds. The Geophysical Instrument Pool Potsdam (GIPP) provided seismic instruments for the temporary networks; these (FDSN codes: 7B 2008–2010; 6C 2009–2010 and 2013–2014; 4B 2008–2009; 5C 2012–2014) are archived at the GEOFON Data Center and can be obtained via the GEOFON website (https://geofon.gfz-potsdam.de/waveform/archive/index.php?type=t). Permanent station waveform data can be obtained through the IRIS DMC (https://ds.iris.edu/SeismiQuery/; TJ: seven stations used here [PMP International (Tajikistan), 2005]; IU: one station used here [Albuquerque Seismological Laboratory (ASL)/USGS, 1988]; GE: one station used here [GEOFON Data Center, 1993]). Focus Humanitarian Assistance and the Norwegian Afghanistan Committee organized the seismometer deployment and logistics and L. R.'s fieldwork in Afghanistan. The Tajik Academy of Sciences organized the logistics in Tajikistan. DAAD supported L. R. and S. A. with travel grants. We thank H. Hartmann, K. Stübner, and M. Tichomirowa for joint fieldwork and the TIPAGE and TIPTIMON groups at GFZ Potsdam and TU Bergakademie Freiberg for technical support and discussions. Many thanks to T. Rautian for interesting discussions on the Garm seismicity. In addition to T. Rautian, we thank D. Simpson, W. Leith, M. Hamburger, and G. Pavlis for their efforts on making the CSE Garm catalog available and their input on these data. We thank A. Robinson and an anonymous reviewer for their very constructive reviews. Most plots were created with the Generic Mapping Tools (GMT; Wessel et al., 2013).

References

Ambraseys, N., & Bilham, R. (2012). The Sarez-Pamir earthquake and landslide of 18 February 1911. *Seismological Research Letters*, *83*(2), 294–314. https://doi.org/10.1785/gssrl.83.2.294

Angelier, J. (1994). Fault-slip analysis and paleostress reconstruction. In P. Hancock (Ed.), *Continental Deformation* (pp. 53–100). Tarrytown, NY: Pergamon.

Avouac, J.-P., Tapponnier, P., Bai, M., You, H., & Wang, G. (1993). Active thrusting and folding along the northern Tien Shan and late Cenozoic rotation of the Tarim relative to Dzungaria and Kazakhstan. *Journal of Geophysical Research*, *98*(B4), 6755–6804. https://doi.org/10.1029/92JB01963

Babaev, A. M. (1975). *Recent tectonics of the zone of orogenesis of the Gissar-Alai and Tajik Depression* (p. 149). Dushanbe: Donish. (in Russian)

Bande, A., Sobel, E. R., Mikolaichuk, A., Schmidt, A., & Stockli, D. F. (2017). Exhumation history of the western Kyrgyz Tien Shan: Implications for intramontane basin formation. *Tectonics*, *36*, 163–180. https://doi.org/10.1002/2016TC004284

Billington, S., Isacks, B. L., & Barazangi, M. (1977). Spatial distribution and focal mechanisms of mantle earthquakes in the Hindu Kush–Pamir region: A contorted Benioff zone. *Geology*, *5*(11), 699–704. https://doi.org/10.1130/0091-7613(1977)5<699:SDAFMO>2.0.CO;2

Bindi, D., Parolai, S., Gómez-Capera, A., Locati, M., Kalmetyeva, Z., & Mikhailova, N. (2014). Locations and magnitudes of earthquakes in Central Asia from seismic intensity data. *Journal of Seismology*, *18*(1), 1–21. https://doi.org/10.1007/s10950-013-9392-1

Bourgeois, O., Cobbold, P. R., Rouby, D., Thomas, J. C., & Shein, V. (1997). Least squares restoration of Tertiary thrust sheets in map view, Tajik depression, central Asia. *Journal of Geophysical Research*, *102*(B12), 27,553–27,573. https://doi.org/10.1029/97JB02477

Brookfield, M. E., & Hashmat, A. (2001). The geology and petroleum potential of the North Afghan platform and adjacent areas (northern Afghanistan, with parts of southern Turkmenistan, Uzbekistan and Tajikistan). *Earth-Science Reviews*, *55*(1-2), 41–71. https://doi.org/10.1016/S0012-8252(01)00036-8

Burtman, V. S. (1975). Structural geology of Variscan Tien Shan, USSR. *American Journal of Science*, *275*(A), 157–186.

Burtman, V. S., & Molnar, P. H. (1993). Geological and geophysical evidence for deep subduction of continental crust beneath the Pamir. *GSA Special Papers*, *281*, 1–76.

Cao, K., Wang, G. C., van der Beek, P., Bernet, M., & Zhang, K. X. (2013). Cenozoic thermo-tectonic evolution of the northeastern Pamir revealed by zircon and apatite fission-track thermochronology. *Tectonophysics*, *589*, 17–32. https://doi.org/10.1016/j.tecto.2012.12.038

Carrapa, B., DeCelles, P. G., Wang, X., Clementz, M. T., Mancin, N., Stoica, M., et al. (2015). Tectono-climatic implications of Eocene Paratethys regression in the Tajik basin of central Asia. *Earth and Planetary Science Letters*, *424*, 168–178.

Chapman, J. B., Carrapa, B., Ballato, C., DeCelles, P. G., Worthington, J., Oimahmadov, I., et al. (2017). Intracontinental subduction beneath the Pamir Mountains: Constraints from thermokinematic modeling of shortening in the Tajik fold-and-thrust belt. *GSA Bulletin*. https://doi.org/10.1130/B31730.1

Chatelain, J. L., Roecker, S. W., Hatzfeld, D., & Molnar, P. (1980). Microearthquake seismicity and fault plane solutions in the Hindu Kush region and their tectonic implications. *Journal of Geophysical Research*, *85*(B3), 1365–1387. https://doi.org/10.1029/JB085iB03p01365

Coutand, I., Strecker, M., Arrowsmith, J., Hilley, G., Thiede, R., Korjenkov, A., & Omuraliev, M. (2002). Late Cenozoic tectonic development of the intramontane Alai Valley (Pamir-Tien Shan region, central Asia): An example of intracontinental deformation due to the Indo-Eurasia collision. *Tectonics*, *21*(6), 1053. https://doi.org/10.1029/2002TC001358

Doebrich, J. L., & Wahl, R. R. (Compilators) (2006). Geological and mineral resource map of Afghanistan; version 2, *U.S. Geological Survey Open-File Report, 2006–1038*.

Dziewoński, A. M., Chou, T.-A., & Woodhouse, J. (1981). Determination of earthquake source parameters from waveform data for studies of global and regional seismicity. *Journal of Geophysical Research*, *86*(B4), 2825–2852. https://doi.org/10.1029/JB086iB04p02825

Eberhart-Phillips, D. (1993). Local earthquake tomography: Earthquake source regions. In H. Iyer & K. Hirahara (Eds.), *Seismic tomography: Theory and practice* (pp. 614–643). London: Chapman and Hall.

Ekström, G., Nettles, M., & Dziewoński, A. M. (2012). The global CMT project 2004–2010: Centroid-moment tensors for 13,017 earthquakes. *Physics of the Earth and Planetary Interiors*, *200-201*, 1–9. https://doi.org/10.1016/j.pepi.2012.04.002

Engdahl, E. R., van der Hilst, R., & Buland, R. (1998). Global teleseismic earthquake relocation with improved travel times and procedures for depth determination. *Bulletin of the Seismological Society of America*, *88*(3), 722–743.

Enkelmann, E., Koons, P. O., Pavlis, T. L., Hallet, B., Barker, A., Elliott, J., et al. (2015). Cooperation among tectonic and surface processes in the St. Elias Range, Earth's highest coastal mountains. *Geophysical Research Letters*, *42*, 5838–5846. https://doi.org/10.1002/2015GL064727

Evans, J. R., Eberhart-Phillips, D., & Thurber, C. (1994). User's manual for SIMULPS12 for imaging vp and vp/vs; a derivative of the "Thurber" tomographic inversion SIMUL3 for local earthquakes and explosions. Technical report, Open File Report 94–431, US Geological Survey.

Evans, S. G., Roberts, N. J., Ischuk, A., Delaney, K. B., Morozova, G. S., & Tutubalina, O. (2009). Landslides triggered by the 1949 Khait earthquake, Tajikistan, and associated loss of life. *Engineering Geology*, *109*(3–4), 195–212. https://doi.org/10.1016/j.enggeo.2009.08.007

Fan, G., Ni, J. F., & Wallace, T. C. (1994). Active tectonics of the Pamirs and Karakorum. *Journal of Geophysical Research*, *99*(B4), 7131–7160. https://doi.org/10.1029/93JB02970

Finzel, E. S., Flesch, L. M., Ridgway, K. D., Holt, W. E., & Ghosh, A. (2015). Surface motions and intraplate continental deformation in Alaska driven by mantle flow. *Geophysical Research Letters*, *42*, 4350–4358. https://doi.org/10.1002/2015GL063987

Forsten, A., & Sharapov, S. (2000). Fossil equids (Mammalia, Equidae) from the Neogene and Pleistocene of Tadzhikistan. *Geodiversitas*, *22*(2), 293–314.

Gągała, L. (2014). Structural geometry and kinematics of the Tajik Depression, central Asia: Neogene basin inversion in front of the pamir salient. Doctoral thesis (161 pp.). TU Bergakademie Freiberg, Germany.

GEOFON (2017). On-line bulletin. http://geofon.gfz-potsdam.de/. GFZ German Research Centre for Geosciences, Potsdam, Germany.

Hacker, B. R., Ratschbacher, L., Rutte, D., Stearns, M. A., Malz, N., Stübner, K., et al. (2017). Building the Pamir-Tibet plateau—Crustal stacking, extensional collapse, and lateral extrusion in the Central Pamir: 3. Thermobarometry and petrochronology of deep Asian crust. *Tectonics*, *36*, 1743–1766. https://doi.org/10.1002/2017TC004488

Hamburger, M. W., Sarewitz, D. R., Pavlis, G. L., & Popandopulo, G. A. (1992). Structural and seismic evidence for intracontinental subduction in the Peter the First Range, central Asia. *Geological Society of America Bulletin*, *104*(4), 397–408. https://doi.org/10.1130/0016-7606(1992)104<0397:SASEFI>2.3.CO;2

Hamburger, M. W., Swanson, W. A., & Popandopulo, G. A. (1993). Velocity structure and seismicity of the Garm region, Central Asia. *Geophysical Journal International*, *115*(2), 497–511. https://doi.org/10.1111/j.1365-246X.1993.tb01202.x

Hu, J., Yang, H., Xu, X., Wen, L., & Li, G. (2012). Lithospheric structure and crust–mantle decoupling in the southeast edge of the Tibetan Plateau. *Gondwana Research*, *22*(3–4), 1060–1067. https://doi.org/10.1016/j.gr.2012.01.003

Hutton, L., & Boore, D. M. (1987). The ML scale in southern California. *Bulletin of the Seismological Society of America*, *77*(6), 2074–2094.

International Seismological Centre (2014). On-line bulletin, http://www.isc.ac.uk, Internatl. Seismol. Cent., Thatcham, United Kingdom.

Ischuk, A., Bendick, R., Rybin, A., Molnar, P., Khan, S. F., Kuzikov, S., et al. (2013). Kinematics of the Pamir and Hindu Kush regions from GPS geodesy. *Journal of Geophysical Research: Solid Earth*, *118*, 2408–2416. https://doi.org/10.1002/jgrb.50185

Jackson, J., Molnar, P., Patton, H., & Fitch, T. (1979). Seismotectonic aspects of the Markansu Valley, Tadjikstan, earthquake of August 11, 1974. *Journal of Geophysical Research*, *84*(B11), 6157–6167. https://doi.org/10.1029/JB084iB11p06157

Käßner, A., Ratschbacher, L., Jonckheere, R., Enkelmann, E., Khan, K., Sonntag, B.-L., et al. (2016). Cenozoic intracontinental deformation and exhumation at the northwestern tip of the India-Asia collision—southwestern Tian Shan, Tajikistan, and Kyrgyzstan. *Tectonics*, *35*, 2171–2194. https://doi.org/10.1002/2015TC003897

Käßner, A., Ratschbacher, L., Pfänder, J. A, Hacker, B. R., Zack, G., Sonntag, B.-L., et al. (2017). Proterozoic-Mesozoic history of the central Asian Orogenic Belt in the Tajik and southwestern Kyrgyz Tian Shan: U-Pb, $^{40}Ar/^{39}Ar$, fission-track geochronology, and geochemistry of granitoids. *Geological Society of America Bulletin*, *129*(3-4), 281–303. https://doi.org/10.1130/B31466.1

Klocke, M., Voigt, T., Kley, J., Pfeiffer, S., Rocktäschel, T., Keil, S., & Gaupp, R. (2015). Cenozoic evolution of the Pamir and Tian Shan mountains reflected in syntectonic deposits of the Tajik Basin. *Geological Society, London, Special Publications*, *427*. https://doi.org/10.1144/SP427.7

Koulakov, I., & Sobolev, S. (2006). A tomographic image of Indian lithosphere break-off beneath the Pamir–Hindukush region. *Geophysical Journal International*, *164*(2), 425–440. https://doi.org/10.1111/j.1365-246X.2005.02841.x

Kuchai, V., & Trifonov, V. (1977). Young left-lateral strike slip along the zone of the Darvaz-Karakul Fault. *Geotektonika*, *3*, 91–105.

Kufner, S. K., Schurr, B., Haberland, C., Zhang, Y., Saul, J., Ischuk, A., & Oimahmadov, I. (2017). Zooming into the Hindu Kush slab break-off: A rare glimpse on the terminal stage of subduction. *Earth and Planetary Science Letters*, *461*, 127–140. https://doi.org/10.1016/j.epsl.2016.12.043

Kufner, S. K., Schurr, B., Sippl, C., Yuan, X., Ratschbacher, L., Ischuk, A., & Tilmann, F. (2016). Deep India meets deep Asia: Lithospheric indentation, delamination and break-off under Pamir and Hindu Kush (Central Asia). *Earth and Planetary Science Letters*, *435*, 171–184. https://doi.org/10.1016/j.epsl.2015.11.046

Kulikova, G. (2016). Source parameters of the major historical earthquakes in the Tien-Shan region from the late 19th to the early 20th century. Doctoral thesis (164 pp.). Germany: University of Potsdam.

Kulikova, G., Schurr, B., Krüger, F., Brzoska, E., & Heimann, S. (2016). Source parameters of the Sarez-Pamir earthquake of 1911 February 18. *Geophysical Journal International*, *205*(2), 1086–1098. https://doi.org/10.1093/gji/ggw069

Leith, W., & Simpson, D. W. (1986a). Earthquakes related to active salt doming near Kulyab, Tadjikistan, USSR. *Geophysical Research Letters*, *13*(10), 1019–1022. https://doi.org/10.1029/GL013i010p01019

Leith, W., & Simpson, D. W. (1986b). Seismic domains within the Gissar-Kokshal seismic zone, soviet central Asia. *Journal of Geophysical Research*, *91*(B1), 689–699. https://doi.org/10.1029/JB091iB01p00689

Lister, G., Kennett, B., Richards, S., & Forster, M. (2008). Boudinage of a stretching slablet implicated in earthquakes beneath the Hindu Kush. *Nature Geoscience*, *1*(3), 196–201. https://doi.org/10.1038/ngeo132

Lomax, A. (2008). The nonlinloc software guide. *ALomax Scientific*, http://alomax.free. fr/nlloc, Mouans-Sartoux, France.

Lukk, A. A., Leonova, V. G., & Shevchenko, V. I. (2008). Seismotectonic characteristics of the northern flank and axial part of the Tajik depression (the Garm geodynamic research area). *Izvestiya Physics of the Solid Earth*, *44*(12), 965–1001. https://doi.org/10.1134/S1069351308120021

Lukk, A. A., & Yunga, S. L. (1988). *Geodynamics and stress strain state of the lithosphere of the central Asia* (p. 234). Dushanbe: Donish.

Lukk, A. A., Yunga, S. L., Shevchenko, V. I., & Hamburger, M. W. (1995). Earthquake focal mechanisms, deformation state, and seismotectonics of the Pamir-Tien Shan region, Central Asia. *Journal of Geophysical Research*, *100*(B10), 20,321–20,343. https://doi.org/10.1029/95JB02158

Mechie, J., Yuan, X., Schurr, B., Schneider, F. M., Sippl, C., Ratschbacher, L., et al. (2012). Crustal and uppermost mantle velocity structure along a profile across the Pamir and southern Tien Shan as derived from project TIPAGE wide-angle seismic data. *Geophysical Journal International*, *188*(2), 385–407. https://doi.org/10.1111/j.1365-246X.2011.05278.x

Metzger, S., Ischuk, A., Zubovich, A., Deng, Z., Schöne, T., Schurr, B., Moreno, M., & Kufner, S.-K. (2018). Observations from four high-resolution GPS profiles across the active margin of the Pamir, Central Asia: Can we discriminate interseismic fault slip-rates, slip partitioning, and even co-seismically triggered slip?, Slip partitioning, and even co-seismically triggered slip? In *EGU General Assembly Conference Abstracts*.

Metzger, S., Schurr, B., Ratschbacher, L., Sudhaus, H., Kufner, S.-K., Schöne, T., et al. (2017). The 2015 M_w7.2 Sarez strike-slip earthquake in the Pamir interior: Response to the underthrusting of India's western promontory. *Tectonics*, *36*, 2407–2421. https://doi.org/10.1002/2017TC004581

Mohadjer, S., Bendick, S. R., Ischuk, A., Kuzikov, S., Kostuk, A., Saydullaev, U., et al. (2010). Partitioning of India/Eurasia convergence in the Pamir-Hindu Kush from GPS measurements. *Geophysical Research Letters*, *37*, L04305. https://doi.org/10.1029/2009GL041737

Molnar, P., & Stock, J. M. (2009). Slowing of India's convergence with Eurasia since 20 Ma and its implications for Tibetan mantle dynamics. *Tectonics*, *28*, TC3001. https://doi.org/10.1029/2008TC002271

Nábēlek, J., & Xia, G. (1995). Moment tensor analysis using regional data: Application to the 25 March, 1993, Scotts Mills, Oregon, earthquake. *Geophysical Research Letters*, *22*(1), 13–16. https://doi.org/10.1029/94GL02760

Negredo, A. M., Replumaz, A., Villaseñor, A., & Guillot, S. (2007). Modeling the evolution of continental subduction processes in the Pamir–Hindu Kush region. *Earth and Planetary Science Letters*, *259*(1–2), 212–225. https://doi.org/10.1016/j.epsl.2007.04.043

Nersesov, I., & Popandopulo, G. (1988). Spatial nonuniformity of time variations of the velocity parameters in the Earth's crust of the Garm region. *Izvestiya of the Academy of Sciences, USSR.: Physics of the Solid Earth*, *24*, 603.

Ni, J. (1978). Contemporary tectonics in the Tien Shan region. *Earth and Planetary Science Letters*, *41*(3), 347–354. https://doi.org/10.1016/0012-821X(78)90189-9

Nikolaev, V. (2002). Afghan-Tajik depression: Architecture of sedimentary cover and evolution. *Russian Journal of Earth Sciences*, *4*(6), 399–421. https://doi.org/10.2205/2002ES000106

Pavlis, G. L., & Das, S. (2000). The Pamir-Hindu Kush seismic zone as a strain marker for flow in the upper mantle. *Tectonics*, *19*(1), 103–115. https://doi.org/10.1029/1999TC900062

Pavlis, T. L., Hamburger, M. W., & Pavlis, G. L. (1997). Erosional processes as a control on the structural evolution of an actively deforming fold and thrust belt: An example from the Pamir-Tien Shan region, central Asia. *Tectonics*, *16*(5), 810–822. https://doi.org/10.1029/97TC01414

Pegler, G., & Das, S. (1998). An enhanced image of the Pamir–Hindu Kush seismic zone from relocated earthquake hypocentres. *Geophysical Journal International*, *134*(2), 573–595. https://doi.org/10.1046/j.1365-246x.1998.00582.x

Roecker, S. W. (1982). Velocity structure of the Pamir-Hindu Kush region: Possible evidence of subducted crust. *Journal of Geophysical Research*, *87*(B2), 945–959. https://doi.org/10.1029/JB087iB02p00945

Ruleman, C. A., Crone, A. J., Machette, M. N., Haller, K. M., & Rukstales, K. S. (2007). *Map and database of probable and possible Quaternary faults in Afghanistan* (no. 2007-1103). Afghanistan: Geological Survey (US).

Rutte, D., Ratschbacher, L., Khan, J., Stübner, K., Hacker, B. R., Stearns, M. A., et al. (2017). Building the Pamir-Tibet Plateau-crustal stacking, extensional collapse, and lateral extrusion in the central Pamir: 2. Timing and rates. *Tectonics*, *36*, 385–419. https://doi.org/10.1002/TC004294

Rutte, D., Ratschbacher, L., Schneider, S., Stübner, K., Stearns, M. A., Gulzar, M. A., & Hacker, B. R. (2017). Building the Pamir-Tibet Plateau-crustal stacking, extensional collapse, and lateral extrusion in the central Pamir: 1. Geometry and kinematics. *Tectonics*, *36*, 342–384. https://doi.org/10.1002/2016TC004293

Sangha, S., Peltzer, G., Zhang, A., Meng, L., Liang, C., Lundgren, P., & Fielding, E. (2017). Fault geometry of 2015, M_w7.2 Murghab, Tajikistan earthquake controls rupture propagation: Insights from InSAR and seismological data. *Earth and Planetary Science Letters*, *462*, 132–141. https://doi.org/10.1016/j.epsl.2017.01.018

Schneider, F. M., Yuan, X., Schurr, B., Mechie, J., Sippl, C., Haberland, C., et al. (2013). Seismic imaging of subducting continental lower crust beneath the Pamir. *Earth and Planetary Science Letters*, *375*, 101–112. https://doi.org/10.1016/j.epsl.2013.05.015

Schurr, B., & Nábělek, J. (1999). New techniques for the analysis of earthquake sources from local array data with an application to the 1993 Scotts Mills, Oregon, aftershock sequence. *Geophysical Journal International*, *137*(3), 585–600. https://doi.org/10.1046/j.1365-246x.1999.00771.x

Schurr, B., Ratschbacher, L., Sippl, C., Gloaguen, R., Yuan, X., & Mechie, J. (2014). Seismotectonics of the Pamir. *Tectonics*, *33*(8), 1501–1518. https://doi.org/10.1002/2014TC003576

Schurr, B., Yuan, X., Haberland, C., & Kufner, S.-K. (2012). *TIPTIMON (Tian Shan-Pamir monitoring program) Tajikistan (2012/2014)*. Germany: Deutsches GeoForschungsZentrum GFZ.

Schurr, B., Yuan, X., Haberland, C., & Kufner, S.-K. (2013). *TIPTIMON (Tian Shan-Pamir monitoring program) Afghanistan (2013/2014)*. Germany: Deutsches GeoForschungs-Zentrum GFZ.

Schwab, M., Ratschbacher, L., Siebel, W., McWilliams, M., Minaev, V., Lutkov, V., et al. (2004). Assembly of the Pamirs: Age and origin of magmatic belts from the southern Tien Shan to the southern Pamirs and their relation to Tibet. *Tectonics*, *23*, TC4002. https://doi.org/10.1029/2003TC001583

Sippl, C., Ratschbacher, L., Schurr, B., Krumbiegel, C., Rui, H., Pingren, L., & Abdybachaev, U. (2014). The 2008 Nura earthquake sequence at the Pamir-Tian Shan collision zone, southern Kyrgyzstan. *Tectonics*, *33*, 2382–2399. https://doi.org/10.1002/2014TC003705

Sippl, C., Schurr, B., Tympel, J., Angiboust, S., Mechie, J., Yuan, X., et al. (2013). Deep burial of Asian continental crust beneath the Pamir imaged with local earthquake tomography. *Earth and Planetary Science Letters*, *384*, 165–177. https://doi.org/10.1016/j.epsl.2013.10.013

Sippl, C., Schurr, B., Yuan, X., Mechie, J., Schneider, F. M., Gadoev, M., et al. (2013). Geometry of the Pamir-Hindu Kush intermediate-depth earthquake zone from local seismic data. *Journal of Geophysical Research: Solid Earth*, *118*, 1438–1457. https://doi.org/10.1002/jgrb.50128

Sobel, E. R., & Dumitru, T. A. (1997). Thrusting and exhumation around the margins of the western Tarim basin during the India-Asia collision. *Journal of Geophysical Research*, *102*(B3), 5043–5063. https://doi.org/10.1029/96JB03267

Sobel, E. R., Schoenbohm, L. M., Chen, J., Thiede, R., Stockli, D. F., Sudo, M., & Strecker, M. R. (2011). Late Miocene–Pliocene deceleration of dextral slip between Pamir and Tarim: Implications for Pamir orogenesis. *Earth and Planetary Science Letters*, *304*(3-4), 369–378. https://doi.org/10.1016/j.epsl.2011.02.012

Spang, J. H. (1972). Numerical method for dynamic analysis of calcite twin lamellae. *Geological Society of America Bulletin*, *83*(2), 467–472. https://doi.org/10.1130/0016-7606(1972)83[467:NMFDAO]2.0.CO;2

Sperner, B. L. A. N. K. A., & Ratschbacher, L. (1994). A Turbo Pascal program package for graphical presentation and stress analysis of calcite deformation. *Zeitschrift der Deutschen Geologischen Gesellschaft*, *145*, 414–423.

Sternai, P., Avouac, J. P., Jolivet, L., Faccenna, C., Gerya, T., Becker, T. W., et al. (2016). On the influence of the asthenospheric flow on the tectonics and topography at a collision-subduction transition zones: Comparison with the eastern Tibetan margin. *Journal of Geodynamics*, *100*, 184–197. https://doi.org/10.1016/j.jog.2016.02.009

Strecker, M. R., Frisch, W., Hamburger, M. W., Ratschbacher, L., Semiletkin, S., Zamoruyev, A., & Sturchio, N. (1995). Quaternary deformation in the eastern Pamirs, Tadzhikistan and Kyrgyzstan. *Tectonics*, *14*(5), 1061–1079. https://doi.org/10.1029/95TC00927

Stübner, K., Ratschbacher, L., Rutte, D., Stanek, K., Minaev, V., Wiesinger, M., et al. (2013). The giant Shakhdara migmatitic gneiss dome, Pamir, India–Asia collision zone, 1: Geometry and kinematics. *Tectonics*, *32*, 948–979. https://doi.org/10.1002/tect.20057

Tapponnier, P., Mattauer, M., Proust, F., & Cassaigneau, C. (1981). Mesozoic ophiolites, sutures, and large-scale tectonic movements in Afghanistan. *Earth and Planetary Science Letters*, *52*(2), 355–371. https://doi.org/10.1016/0012-821X(81)90189-8

Teshebaeva, K., Sudhaus, H., Echtler, H., Schurr, B., & Roessner, S. (2014). Strain partitioning at the eastern Pamir-Alai revealed through SAR data analysis of the 2008 Nura earthquake. *Geophysical Journal International*, *198*(2), 760–774. https://doi.org/10.1093/gji/ggu158

Thomas, J. C., Chauvin, A., Gapais, D., Bazhenov, M. L., Perroud, H., Cobbold, P. R., & Burtman, V. S. (1994). Paleomagnetic evidence for Cenozoic block rotation in the Tajik depression (central Asia). *Journal of Geophysical Research*, *99*(B8), 15,141–15,160. https://doi.org/10.1029/94JB00901

Thomas, J. C., Cobbold, P. R., Wright, A., & Gapais, D. (1996). Cenozoic tectonics of the Tadzhik depression, central Asia. In A. Yin & M. Harrison (Eds.), *The tectonic evolution of Asia* (pp. 191–210). Cambridge: Cambridge University Press.

Thomas, J. C., Gapais, D., Cobbold, P. R., Meyer, V., & Burtmann, V. S. (1994). Tertiary kinematics of the Tadjik depression (central Asia): Inferences from fault and fold patterns. In F. Roure, et al. (Eds.), *Geodynamic evolution of sedimentary basins* (pp. 171–180). Moscow.

Thompson, J. A., Burbank, D. W., Li, T., Chen, J., & Bookhagen, B. (2015). Late Miocene northward propagation of the northeast Pamir thrust system, northwest China. *Tectonics*, *34*, 510–534. https://doi.org/10.1002/2014TC003690

Thurber, C. (1983). Earthquake locations and three-dimensional crustal structure in the Coyote Lake area, central California. *Journal of Geophysical Research*, *88*(B10), 8226–8236. https://doi.org/10.1029/JB088iB10p08226

Thurber, C. (1993). *Local earthquake tomography: Velocities and V_P/V_S*-theory (pp. 563–583). Chapman and Hall, London: Seismic tomography: Theory and practice.

Treloar, P. J., & Izatt, C. N. (1993). Tectonics of the Himalayan collision between the Indian plate and the Afghan block: A synthesis. *Geological Society, London, Special Publications*, *74*(1), 69–87. https://doi.org/10.1144/GSL.SP.1993.074.01.06

Trifonov, V. G. (1978). Late Quaternary tectonic movements of western and central Asia. *Geological Society of America Bulletin*, *89*(7), 1059–1072. https://doi.org/10.1130/0016-7606(1978)89<1059:LQTMOW>2.0.CO;2

USGS (2017). USGS earthquake bulletins, on-line bulletin. http://earthquake.usgs.gov/. United States Geological Survey.

van Hinsbergen, D. J., Kapp, P., Dupont-Nivet, G., Lippert, P. C., DeCelles, P. G., & Torsvik, T. H. (2011). Restoration of Cenozoic deformation in Asia and the size of Greater India. *Tectonics*, *30*, TC5003. https://doi.org/10.1029/2011TC002908

van Hunen, J., & Allen, M. B. (2011). Continental collision and slab break-off: A comparison of 3-D numerical models with observations. *Earth and Planetary Science Letters*, *302*(1-2), 27–37. https://doi.org/10.1016/j.epsl.2010.11.035

Vlasov, N. G., Dyakov, Y. A., & Cherev, E. S. (1991). Geological map of the Tajik SSR and adjacent territories, 1:500,000, Leningrad.

Waldhauser, F. (2001). hypoDD—A program to compute double-difference hypocenter locations. Technical report, open file report 94–431, 01-113, 25 pp., US Geological Survey.

Waldhauser, F., & Ellsworth, W. L. (2000). A double-difference earthquake location algorithm: Method and application to the northern Hayward fault, California. *Bulletin of the Seismological Society of America*, *90*(6), 1353–1368. https://doi.org/10.1785/0120000006

Wang, P., Scherler, D., Liu-Zeng, J., Mey, J., Avouac, J. P., Zhang, Y., & Shi, D. (2014). Tectonic control of Yarlung Tsangpo Gorge revealed by a buried canyon in southern Tibet. *Science*, *346*(6212), 978–981. https://doi.org/10.1126/science.1259041

Wessel, P., Smith, W. H., Scharroo, R., Luis, J., & Wobbe, F. (2013). Generic mapping tools: Improved version released. *Eos, Transactions American Geophysical Union*, *94*(45), 409–410. https://doi.org/10.1002/2013EO450001

Whipp, D. M., Beaumont, C., & Braun, J. (2014). Feeding the "aneurysm": Orogen-parallel mass transport into Nanga Parbat and the western Himalayan syntaxis. *Journal of Geophysical Research: Solid Earth*, *119*, 5077–5096. https://doi.org/10.1002/2013JB010929

Zeitler, P. K., Koons, P. O., Hallet, B., & Meltzer, A. S. (2015). Comment on "Tectonic control of Yarlung Tsangpo Gorge revealed by a buried canyon in southern Tibet". *Science*, *349*(6250), 799–799. https://doi.org/10.1126/science.aaa9380

Zubovich, A., Schöne, T., Metzger, S., Mosienko, O., Mukhamediev, S., Sharshebaev, A., & Zech, C. (2016). Tectonic interaction between the Pamir and Tien Shan observed by GPS. *Tectonics*, *35*, 283–292. https://doi.org/10.1002/2015TC004055

Zubovich, A. V., Wang, X.-Q., Scherba, Y. G., Schelochkov, G. G., Reilinger, R., Reigber, C., et al. (2010). GPS velocity field for the Tien Shan and surrounding regions. *Tectonics*, *29*, TC6014. https://doi.org/10.1029/2010TC002772